Effect of Flagella Like Surface Heterogeneity on The Motion of Charged Macromolecules in The Fibrous Pore

by
Tariq Mahbub
Student No.: 0411102042

Under the supervision of
Dr. Noor Al Quddus

Submitted in partial fulfillment of the requirements for the degree of
MASTER OF SCIENCE IN MECHANICAL ENGINEERING

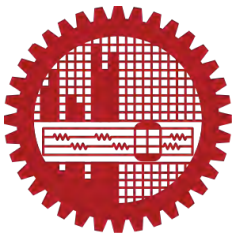

Department of Mechanical Engineering
BANGLADESH UNIVERSITY OF ENGINEERING AND TECHNOLOGY
Dhaka 1000, Bangladesh

June, 2014

This thesis titled **Effect of Flagella Like Surface Heterogeneity on The Motion of Charged Macromolecules in The Fibrous Pore**, submitted by Tariq Mahbub, Student No. 0411102042 Session April 2011 has been accepted as satisfactory in partial fulfillment of the requirement for the degree of MASTER OF SCIENCE IN MECHANICAL ENGINEERING on June 22 , 2014.

BOARD OF EXAMINERS

1. _____ Chairman
Dr. Noor Al Quddus (Supervisor)
Associate Professor,
Department of Mechanical Engineering
Bangladesh University of Engineering and Technology
Dhaka-1000, Bangladesh.

2. _____ Member
Dr. Md. Zahurul Haq (Ex-Officio)
Professor and Head,
Department of Mechanical Engineering
Bangladesh University of Engineering and Technology
Dhaka-1000, Bangladesh.

3. _____ Member
Dr. Mohammad Ali
Professor,
Department of Mechanical Engineering
Bangladesh University of Engineering and Technology
Dhaka-1000, Bangladesh.

4. _____ Member
Dr. A.B.M. Toufique Hasan
Associate Professor,
Department of Mechanical Engineering
Bangladesh University of Engineering and Technology
Dhaka-1000, Bangladesh.

5. _____ Member
Dr. Dewan Hasan Ahmed (External)
Associate Professor,
Department of Mechanical and Production Engineering
Ahsanullah University of Science and Technology
Tejgaon, Dhaka, Bangladesh.

CANDIDATE'S DECLARATION

It is hereby declared that this thesis or any part of it has not been submitted elsewhere for the award of any degree or diploma.

Signature of the candidate

_____

Tariq Mahbub

CERTIFICATE OF RESEARCH

This is to certify that the work presented in this thesis is carried out by the author under the supervision of Dr. Noor Al Quddus, Associate Professor of the Department of Mechanical Engineering, Bangladesh University of Engineering and Technology, Dhaka, Bangladesh.

Dr. Noor Al Quddus

Tariq Mahbub

Dedicated to My Parents

ACKNOWLEDGMENT

At the beginning i would like to express my gratefulness to all mighty Allah to enable me to carry on my endeavor through graduate study. I would also extend my gratefulness to my parents and siblings for their continual support and encouragement.

I must to express my heartiest gratitude to my supervisor Dr. Noor Al Quddus who has guided me through the course of my graduate study and research. Without his guidance, support and suggestion this thesis was simply unthinkable to complete. He has drawn my attention to various aspects of fluid mechanics and motivated me for the fundamental research work. He encouraged me to roam around the vast field of fluid mechanics relevant to my thesis work and showed me the path when got stuck. I have benefitted enormously from our many discussions and his huge engagement in his students.

I want to extend my personal gratification to Mr. Noman Hasan for his continual support and aid regarding current research survey and review of the contemporary works as well as previous literature. I also like to thank Raziya Sultana for her motivation that always push me throughout this thesis work.

ABSTRACT

Motion of a charged particle inside an electrolyte filled uncharged channel is hindered due to hydrodynamic effect and electrokinetic effects. Presence of an obstacle on wall surface increases the drag force on the particle and reduces the particle velocity. Flagellum like obstacle tends to shift the particle away from the center. When any or both the particle and flagellum are charged different electrokinetic phenomena like repulsion, relaxation, electrical double layer overlap affect the drag force on the particle. Electrostatic repulsion always force the particle away from the flagellum if both the particle and flagellum are similarly charged and vice versa. Distortion of electric double layer causes relaxation which always tends of increase the drag force in flow direction. Double layer overlap also affects the drag by redistributing the charge concentration. A finite element model consisting of Navier-Stokes, Poisson and Nernst-Plank equation has been developed to quantify the effect of such parameters on particle drag force. It is found that presence of flagellum hydrodynamically tends to offcenter the particle at flagellum upstream and later brings it back. Relaxation more prominently affects electrical drag force than electrostatic repulsion and increases the drag force on the stationary particle in flow direction. With the decrease of separation distance both the hydrodynamic and electrical drag force increase. Solution concentration has significant effect on the drag force. With the increase of concentration electrical drag force increases significantly due to increased surface charge on the particle surface resulting in higher total drag force. Drag factor has been found to be higher for charged particle than uncharged one. This excess drag is also increases with solution concentration.

Contents

NOMENCLATURE

Notation	Definition
α	Scaled axial distance between particle center and flagellum axis
β	Scaled separation distance
ϵ	Permittivity of medium
ϵ_0	Permittivity of vacuum
κ	Debye length
λ	Size ratio, (a/b)
μ	Viscosity of fluid
ρ	Density of fluid
ρ_f	Space charge density
ψ	Electric potential
a	Particle radius
b	Channel radius
D	Diffusivity
e	Fundamental charge
$\mathbf{E}$	Electric field
F	Drag force
h	Separation distance
$\mathbf{I}$	Identity matrix
K_1, K_2	Drag factor
k_B	Boltzmann constant
L_f	Length of flagellum
n	Ion concentration
P	Pressure
T	Absolute temperature
$\mathbf{u}$	Velocity vector
v_{max}	Maximum fluid velocity
X, Y, Z	Coordinate axis
z	Valency of ion
Superscript (*)	Scaled quantity
Subscript (p)	Positive ion
Subscript (n)	Negative ion
Subscript (∞)	Bulk properties
Subscript (e)	Electrical properties
Subscript (h)	Hydrodynamic properties
Subscript (t)	Total quantity

List of Figures

List of Tables

Chapter 1

INTRODUCTION

1.1 Background and Motivation

Numerous engineering applications involve fluid flow containing suspended charged particles and require particle filtration. The diversity of such applications may be illustrated by a few examples: membrane filtration, the characterization of hemodialysis membranes, the modeling of size-exclusion and hydrodynamic chromatography, the determination of an optimal pore size for supported catalysts, DNA and protein separations, porous media flow and blood flow modeling [20][3] [11] as in Fig: 1.1. To understand the separation technique of these filtration membranes, the hindered transport theory has been extensively investigated. It is well known that solutes in liquid filled pores of molecular dimensions have reduced diffusivities. For large solute molecules that are in the order of channel radius in size, this hindered transport can be explained by a combination of the particle-wall hydrodynamic and electrokinetic interactions and steric restrictions. This phenomenon has been studied both theoretically and experimentally in past, to understand the effect of size of the solute particles on membrane permeability.

The description of membrane transport in terms of a series of parallel pores of cylindrical shapes has received considerable attention over the years. Modeling the pores as the summation of parallel cylinders has significant benefit as it requires only analyzing the problem of a single particle in a single cylindrical channel. The fundamental research on the hydrodynamic interaction of spherical particle moving through liquid filled channel is comprehensively investigated in the past.The effect of the vicinity of the wall on the particle motion is usually characterized in terms of dimensionless wall correction factors and lag factor. Wall correction factor is the ratio of the drag force encountered by a moving particle through a liquid filled

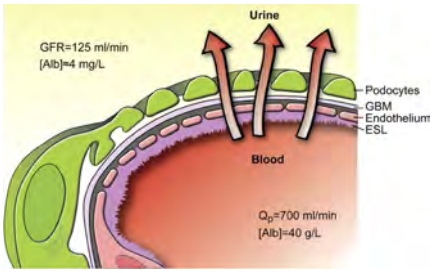

(a) Renal filtration membrane

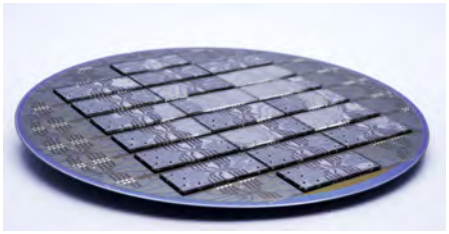

(b) Lab-on-Chip device

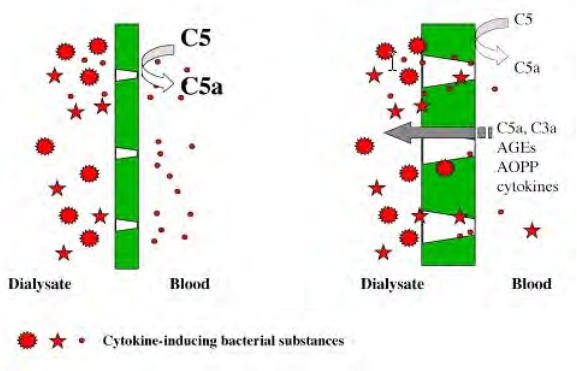

(c) Hemodialysis membrane

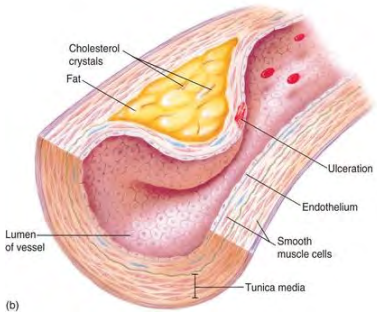

(d) Atherosclerosis

Figure 1.1: Various applications of charged particle motion through confined channel

channel to the drag force experienced when moving through unbounded liquid. Lag factor is the ratio of the steady velocity of particle to the velocity of the fluid in absence of particle. This defines how slow a particle moves relative to the flowing fluid.

Although the theory of hindered transport for a particle moving in a cylindrical pore is very well studied, most of the analyses considered the centerline approximation i.e. the particle will remain at the centerline of the pore[13][16]. Ferry[21] first derived hindrance factor for convection from steric consideration to explain the selectivity of porous membrane. Hydrodynamic terms were introduced to describe the reduction in solute mobility within pores[37]. However, in these studies mentioned above, only hydrodynamic effect of the pore wall was considered neglecting any electrokinetic effect[1]. A common approach to address the effect of charged pore is to assume a very thin electric double layer. The effect of the double layer on the flow field is then introduced by allowing a slip boundary condition on the particle surface and the particle mobility calculated by employing the method of reflection[28][19]. Filtration phenomena were later assessed by fibrous membrane model[5] and periodic fiber array[51]. Electrokinetic studies also consider the centerline approximation and a uniform pore. But in actual case uniform pore is hard

to find and the charged object like, DNA, protein, colloids can assume any radial position.

Further more along with thin double layer, Poisson Boltzmann equation was used to explain the potential distribution inside EDL. As a result distortion in EDL caused by the flow and EDL overlap could not be computed exactly. Recently coupled Poisson and Nernst-Plack equation was employed to evaluate these effects on hindered diffusivity [15]. But these studies also considered uniform pore. Motivated by the lacking of hindered motion of charged particle inside pore having charged surface heterogeneity in literature, in this thesis a 3D finite element model is developed to deal with surface heterogeneity for hindered motion of charged particle.

A three dimensional finite element model has been developed to study the drag force for a charged macromolecule moving thorough a long pore containing flagellum like charged obstacle on the surface. The model uses Navier-Stokes, continuity, Poisson and Nernst-Plank equations and employs plausible boundary conditions to solve the computational domain. Complete form of Navier -Stokes equation dictates the flow field inside then pore and around the particle and allows to consider inertia, viscous and electrokinetic forces. Nernst-Plank equation deals with the charge distribution throughout the channel though convection and diffusion and enables the Poisson equation to determine the potential distribution across the channel. In coupled form this PNP-NS model can evaluate the complex state of distorted electric double layer caused by distortion and overlap. The set of nonlinear equations have been solved in a finite element package in coupled manner to obtain velocity and pressure fields, potential and concentration distributions. Total drag force is obtained by integrating viscous stress and Maxwell stress tensor over the particle. These forces later used to calculate drag factor.

1.2 Objectives of the Thesis

The specific objectives of the thesis work are as follows:

- To develop a 3-D finite element model consisting of Navier-Stokes, continuity, Poisson and Nernst-Planck equations to study the motion of rigid, charged spherical particle moving through heterogeneous cylindrical pore.
- To validate the 3-D finite element model with established solution of linearized Navier-Stokes, continuity, Poisson and Nernst-Planck equations.

- To study the effect of charged flagellum of different length at the channel wall on the motion of the particle of different size ratio at different solute concentration.
- To calculate the mobility of spherical particle moving in the heterogeneous pore and the excess drag produced by the presence of charge flagellum.

1.3 Outline of the Thesis

A detail literature review is provided in Chapter 2. The theoretical description of the model is described in Chapter 3. The particle-channel geometrical configuration, the governing equations for fluid flow, electric field distribution and ion distribution, boundary conditions, non-dimensionalization of the model, and calculation procedure of wall correction factors are described. Chapter 4, presents the simulation results. First the model is validated by comparing the calculated wall correction factor (K_2) of a spherical particle flowing along the channel axis, against existing analytical and numerical results found in the literature. Then flow profile in a cylindrical channel having charged wall under the application of pressure is compared with the published result. Later another validation is done by comparing the excess drag caused by the presence of charge on spherical particle with the value available in literature. Mesh sensitivity test is also performed. In the later sections, the values of the drag forces are presented for spheres of different sizes, moving through the centerline inside the channel at different flagellum length, surface charge density and solute concentration. Excess drag factor is also calculated. In Chapter 5, the conclusion and the recommendations for future works are presented.

Chapter 2

LITERATURE REVIEW

Motion of a colloidal particle inside pore having diameter of same order of the colloid is of prime interest in the field of hindered transport due to their numerous applications e.g. capillary flow, micro drug delivery, Lab-on-Chip devices, microfilter and many others [34] [36] [10]. The maximum achievable flux for particle-containing fluid through microscopic channel is found significantly less than the pure fluid flux. The rate of convective transport of the solute particles is found to be lower than the product of bulk solute concentration and fluid flow rate. In absence of channel fouling, this hindered transport results entirely from the hydrodynamic retardation effect on the moving particle due to the proximity of wall while the particle and channel both are uncharged. If both the particle and channel wall or any one of them are charged electrokinetic retardation also affect the hindered transport along with hydrodynamic retardation effect. Extensive studies on this topic by different researchers are reviewed in literature [40][24][27].

The first observation of colloidal motion was documented by Robert Brown in 1827 while he was studying the erratic motion of particles in pollen grains suspended in water.Almost hundred years later Einstein in 1905 derived that, the diffusivity of colloid in an unbounded liquid equals the thermal fluctuation energy divided by the drag coefficient [1]. For a spherical solute, the result is the famous Stokes-Einstein equation. With the improvement of optical microscopy experimental observation of colloidal system dynamics boosted up.

An important discovery was made by Reuss in 1809 is that, naturally occurring colloids are charged, incorporating the electrokinetic effect in colloidal system. Later Schulz and Hardy elucidated the role of added electrolytes in suppressing the effect of charge and promoting coagulation providing strong evidence that stability of

aqueous dispersion derived from electrostatic repulsion. A major contribution to the early theoretical development of electrokinetic phenomena was done by Helmholtz and Smoluchowski. In 1903 Smoluchowski presented the celebrated formula relating the surface potential (zeta potential) to the electrophoretic mobility. Helmholtz introduced the theory of Electric Double Layer (EDL). Later improved theory for EDL was independently published by Gouy and Chapman. In all the aforementioned development, electrostatic repulsion was considered only leaving the attractive force caused by Van der Waals interaction between colloidal particles. The first formal theory of colloidal stability was presented independently by Derjaguin and Landau from Soviet Union in 1941 and Verwey and Overbeek from Netherlands in 1948. They expressed the total interparticle interaction as a linear combination of Van der Waals and electrostatic interactions between a pair of particles. This theory is known as DLVO theroy and has formed the basis of modern theoretical colloidal science.

Different theoretical methods have been introduced to explain this hindered transport phenomena. It was an established method to model the pores as the summation of parallel cylinders. As a result, in most of the cases, the motion of a single particle in a cylindrical channel is analyzed. Another simplification is done by assuming the particle motion to be along the axis of the cylinder that reduces the problem from three dimensional analysis to two dimensional axi-symmetric analysis. The effect of proximity of the cylinder walls on the drag of an axially moving sphere was initially analyzed using the method of reflection [23]. In this method, starting with the known solution for the drag of a rigid sphere in an unbounded medium i.e. the Stokes solution, a reflection flow is superposed such that the boundary conditions on the sphere are satisfied exactly. The drag of the sphere is obtained from Stokes law using the velocity of the sphere increased by the average reflection velocity on the sphere. Approximate expression for the drag of the rigid sphere was given.

An exact solution for the wall correction factors for the axial motion of rigid spheres in stationary and moving liquids within an infinitely long cylindrical channel has been obtained in terms of an infinite set of linear algebraic equations for the coefficients of Stokes stream functions [22]. In this analysis, it was pointed out that, the drag of a sphere in motion within a moving liquid is composed of two parts: namely, the drag due to the motion of the sphere in a quiescent liquid inside the cylindrical tube, and the drag due to the motion of the liquid within the cylindrical tube. Both cases were analyzed for rigid spheres and fluid spheres (i.e. spheres which have different physical properties than the external fluid and are character-

ized by internal motion). However, the provided solution for the fluid spheres was approximate. Moreover, the results of the wall correction factors of particles they provided were limited to the ratios of particle to channel radii $\lambda \leq 0.8$, where $\lambda = a/b$ and a and b are the particle and channel radii, respectively.

Singular perturbation techniques was used to investigate the slow, asymmetric flow around a sphere positioned eccentrically within a viscous liquid filled long, circular, cylindrical channel [9]. They provided wall correction factors for the axially flowing spherical particle accurately for all λ values ($0 \leq \lambda \leq 1$). The obtained results covered the situations in which the sphere occupies virtually the entire cross section of the cylinder, so that the clearance between the particle and tube wall was everywhere small compared with both the sphere and tube radii which eventually presented an improved version of the conventional lubrication-theory analysis. Asymptotic expansions, valid for small dimensionless clearances were obtained for the hydrodynamic force, torque and pressure drop for flow past a stationary sphere, and for a sphere translating or rotating in stationary fluid. However, the dependence of drag force on the spherical particle upon its lateral position was represented by an undetermined function. Change in the translational velocity for a sphere in a Poiseuille flow with its eccentric position was predicted. It was stated that, displacement of the sphere to eccentric position decreases its velocity only slightly, unless eccentricity is very close to unity. The sphere translates faster than the mean fluid velocity for most eccentric positions. Lateral displacement of the sphere from the concentric position leads to a considerable increase in additional pressure drop, all other things being equal. Sedimentation of a sphere in a vertical tube was also analyzed. It was found that, the settling velocity increases monotonically with lateral position until the eccentricity equals to 0.98.

First numerical investigation of this topic was initially performed using the finite element method to calculate the wall correction factors for single particle and short chain of particles flowing along the axis of the cylinder [7]. The values of the wall correction factors were obtained for $\lambda \leq 0.8$. Limiting particle spacing for short chain of particles was found, for which single sphere approximation gives accurate results for the inner spheres of the particle chain. It was shown that, single sphere calculations have a wide range of applicability, which simplifies the effort involved in numerical calculations considerably. The calculated values of the wall correction factors were used to evaluate the maximum achievable flux of a particle containing fluid through a micro-porous membrane. In extension of this analysis, the same researchers have included the electrostatic effect with the pure hydrodynamic re-

tardation effect to find the forces on a charged spherical particle as a function of distance of approach and entry to a charged cylindrical channel in a charged planar surface [8]. Galerkin finite element scheme was implemented for getting the numerical solution of the nonlinear Poisson-Boltzmann and Navier-Stokes equations for electrostatic interaction and hydrodynamic interaction, respectively.

The resistance force for a torque free spherical particle flowing eccentrically inside a cylindrical channel was first analyzed numerically [25]. Stokes equation with the boundary conditions was formulated using the boundary integral method. The boundary integral equation was numerically solved by spectral boundary element method. They have considered rigid solid spheres, fluid droplets and bubbles. A lubrication theory was also presented for predicting the limiting resistance of bodies near contact with the cylindrical walls. The calculated numerical data was represented by algebraic expressions for entire eccentricity values ($0 < e < 1$) and for all particle sizes ($0 < \lambda < 0.9$). The numerical coefficients in these algebraic expressions were obtained from the detailed computational results together with known asymptotic limits.

Numerical and asymptotical investigations were performed on the influence of uniform and Poiseuille flow on the wall correction factor of spherical particle placed at the axis of the channel [4]. The Stokes and continuity equations were expressed in terms of the stream function and vorticity formulation and were solved using finite difference method. In all the numerical computations they have calculated the separate contributions of the pressure and viscosity forces. This calculation was in good agreement with those obtained by asymptotic expansions. They have pointed out the prevalence of the pressure term over the viscosity term in the lubrication regime (very high λ values) which is opposite to what happens for dilute regime. The calculated wall correction factors covered the entire range of particle sizes, i.e. $0 < \lambda < 1$.

A finite element particle transport model consisting of Navier-Stokes and continuity equations defined in arbitrary Lagrangian Eulerian kinematics was employed to describe the axial motion of a rigid uncharged spherical particle in an infinitely long cylindrical channel of uniform cross-section [40]. Wall correction factors were calculated covering the entire particle size range ($0 < \lambda < 1$). Finite channel length effects on the motion of the particle were also investigated. These are particle transport at the channel entry and the exit from the reservoir and motion of a particle in a dead end under the influence of an external force. This model directly provides

the lag factor G which is a unique feature of it, as the lag factor was previously determined separately by calculating the wall correction factors. Therefore, this model provides a self consistent solution of the particle transport in the cylindrical capillary including the complete hydrodynamic interactions between the particle and channel wall.

Most of the studies cited above are for uncharged particle inside an uncharged pore rendering the analysis purely hydrodynamic. Similar development also took place in the field of electrokinetic motion of charged colloidal particle inside charged or uncharged channel. This field has numerous implications in different chemical, biological and industrial processes like Chromatography, capillary electrophoresis, filtration, separation and mixing etc. The early development in the theory of motion of charged colloid by Helmholtz, Smoluchowski, Gouy, Chapman and many others have already been discussed.

With the development of Track Etch technology at early 1970 there was a renewed interest in the theory of molecular motion through fine pore. This technology provided an opportunity to directly test the theoretical predictions in model membrane having precisely known properties. Bean [2] and Anderson and Quinn [41] reviewed existing methods of hindered transport and extended the theories in important ways. The most significant contribution they made is the validation of the use of continuum hypothesis in studying the motion of particle both charged and uncharged through small pores. They experimentally showed that viscosity of water doesn't change significantly in pores of molecular dimension. This provided the base of today's theoretical and numerical study of colloidal motion through micro and nano pores.

The electrostatic double layer interaction between a colloidal particle and a long cylindrical pore is theoretically investigated [48]. This was a modification of a previous work done by the same authors where they calculated the potential energy of interaction for a spherical colloid residing at the centerline of a charged pore [47]. Here the colloid could take any position inside the pore resulting in potential energy of interaction at any position of the pore. The equilibrium partitioning coefficient which is the ration of solute concentration at pore to bulk solution was calculated using this interaction energy. Gouy Chapman diffuse double layer model was considered to model the double layer and linearized Poisson-Boltzmann equation was employed to obtain the potential distribution inside the pore. Two other important assumptions were, the solution was very dilute and the channel was infinitely long.

Convection of rigid, spherical solute through cylindrical pore was studied using hydrodynamic model that include both steric and electrostatic interaction between pairs of solute particle and between solute and pore walls [33]. Most of the previous studies of were concerned with totally impermeable and focused on convective diffusion associated with concentration polarization that occur at the upstream side of the membrane. Here a semipermeable membrane is adopted to study the factors that affect rejection coefficient that is the ration of solute concentration at filtrate to retentate. Assuming the solution to be infinitely dilute is many times unacceptable in ultrafiltration. As a result the Boltzmann distribution to evaluate the radial concentration profile inside the pore become unacceptable. To account this Anderson and Brannon using statistical thermodynamics express the radial concentration profile as a virial expansion of bulk concentration. Here Mitchell and Deen used the same technique used by Anderson and Brannon to determine the radial concentration distribution and focused their attention to study the effect of charge on reflection coefficient.

An extensive review on the hindered transport of macro molecules in liquid filled pore was performed by Deen [16]. Diffusive and convective transport of dilute solution of neutral sphere with various extensions like electrostatic interaction, other pore shape, non spherical solute, finite concentration were discussed critically. Different experimental results available were also discussed.

Gibbs ensemble Monte Carlo Simulation technique was used to study the partitioning coefficient between slit pores and bulk solution [12]. This method provides better result for complicated geometry and cases where colloidal interaction can not be avoided. Other methods like virial expansion or density function method showed poorer prediction than this technique. It clearly shows that even at lower concentration the electrostatic interaction between the solutes is more than the compensation by wall-solute interaction and increases the partitioning coefficient indicating that concentration effect must be considered at lest as important as electrostatic effect in determining partitioning coefficient. A systematic approach based on Boundary integral method was developed to yield an approximate analytical expression for various types of shape under a general surface condition for electrical interaction energy between two objects [26].

Separation of protein using charged ultrafiltration membrane was performed experimentally to support the existing theory of hindered transport [35]. It was demonstrated that the rejection ratio for negatively charged Myoglobin is around 80% while

Cytochrome C is completely permitted to pass through negatively charged membrane. Similar experimental studies of size exclusion chromatography and membrane ultrafiltration were performed in parallel using both natural Dextrans and charged proteins [39].

The implication of electrostatic interaction in golmerular filtration has been studied for a long time. Recently [17] on a commentaries describe the implication of Endothelium in renal filtration which was considered to be less till then. A detailed study on the structure of glomerular barrier, effect of each part on filtration, effect of size, shape and charge on restriction of solute in barrier is done [24] based on the present filtration data and microscopic image of glomerular barrier.

The effect of charge on pore and particle on osmotic reflection coefficient [6], intrapore diffusivity [15] and sieving coefficient and lag factor [14] was studied. For the very first time the effect of distorted double layer or relaxation and streaming potential in these factors are studied. Perturbation expansion method was used and FEM was used to solve the set of equations.

Hindered motion of charged macromolecules through charged pore is well studied in literature. Recently electrokinetic phenomena like relaxation, streaming potential, electric double layer (EDL) overlap are also considered along with hydrodynamic forces, steric inclusion, electrostatic repulsion to evaluate the force acting on the particle and different flow and filtration characteristics. But most of the studies used linear Poisson Boltzmann equation, and Stokes equation to evaluate the properties. As a result the complex dynamics of relaxation and EDL overlap stay unexplored. Using Stokes equation make the problem insensitive to inertial interaction. More over not a single study is done to elucidate the effect of presence of a charged flagellum like obstacle inside the pore. This kind of obstacle is quite common in nature like Atherosclerosis, particle deposition in microchannel, gel electrophoresis etc. seeking a clear understanding of particle motion inside channel with charged obstacle at wall. In this thesis three dimensional numerical model is developed using full Navier-Stokes equation to consider the effect of inertia, coupled Poisson, Nernst-Planck equation to take in account the non liner nature of EDL. Above all the the three dimensional geometry of the modle enables it to consider any shape of particle and obstacle. This model can be used to evaluate different forces acting on the particle and drag factors.

Modeling blood flow through blood vessels plays a key role in understanding several aspects of several diseases that hindered blood flow through blood vessel. Various theoretical model had been developed to explain blood flow specially the motion of Red blood cell (RBC) through capillaries [43][44]. In these models axisymmetric cell shapes are assumed, and lubrication theory is used to describe the flow of the suspending fluid in the gaps between the cells and the vessel wall. These models took into account the elastic properties of the red blood cell membrane, including its responses to shear and bending. The drawbacks these model had is, they considered no interaction between RBC and the cells were assumed to flow in a single file. To consider the elastic properties of RBC and Fahraeus-Lindqvist effect a simple two layer model had been developed [45]. This model considered the non-continuum behavior of blood near the vessel wall. Numerical model was also developed to determine the tank-treading motion of the cell wall in high viscous flow[46]. These models predicted the deformation and motion of RBC inside capillary and its bifurcations more or less accurately when compared to experimental observations. Recently with the high increment of computational power 3D models are developed to analyze the actual behavior of RBC in blood flow [18][38][30]. Surprisingly none of these models considered the implication of presence of a net negative charge on the wall of RBC. Actually a few studies were performed to enlighten the effect of charge on the motion of RBC in blood flow. It was found that the presence of charge on the RBC wall reduces its velocity[49]. Study has been also performed to manipulate the motion of RBC using alternating current field[32].

Chapter 3

MATHEMATICAL MODEL

3.1 Fluid drag

Drag or fluid drag refers to the force acting opposite to the motion of any object moving in a fluid. When any object starts to move through any liquid no slip condition on the object causes the fluid adjacent to it, to move along with it. This results in a relative motion in different layers of fluid and viscosity comes into action, trying to resist any kind of relative motion. This creates a resisting force (fluid drag) against the motion of the object and tries to slow down the object. If the object is stationary and fluid is flowing over it, fluid tries to drag the particle along with it.

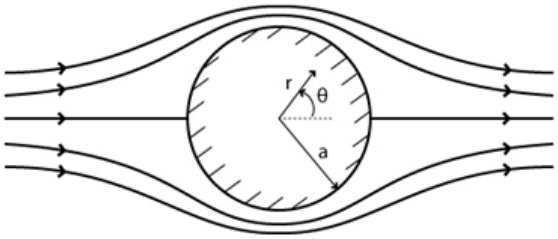

Figure 3.1: Creeping flow over spherical particle

To calculate the drag force let us consider a stationary spherical particle of radius a over which a fluid of density ρ is flowing. It is clear that the approaching fluid must both move faster and be displaced laterally as it flows past the sphere. On the other hand, the no-slip condition requires that the fluid velocity be zero everywhere at the surface of the sphere; this implies the existence of gradients (that is, spatial rates of change) of velocity, very sharp at and near the surface of the sphere. These velocity gradients produce a shear stress on the surface of the sphere.In cylindrical

coordinate (r, θ) the equation of shear stress can be written as [50] ,

$$\tau_{r\theta} = \mu(\frac{1}{r}\frac{\delta u_r}{\delta \theta} + \frac{\delta u_\theta}{\delta r} - \frac{u_\theta}{r}) \tag{3.1}$$

where, $\tau_{r\theta}$= shear stress, μ= viscosity of fluid, $\mathbf{u}(= u_r, u_\theta)$= fluid velocity
Integrating the stress over the surface, the shear force (drag force) exerted by the fluid on the sphere can be obtained. This part of the total drag force on the sphere called the viscous drag. It is understandable that the pressure of the fluid is greater on the front of the sphere than on the back. The sum of the pressure forces over the entire surface of the sphere represents the other part of the drag force, called the pressure drag or form drag. The local pressure(P) on the particle surface is given by, [50]

$$P = P_\infty - \frac{3\mu a \mathbf{u}}{2r^2}\cos\theta \tag{3.2}$$

where, P_∞= uniform free stream pressure, a= sphere radius.
Adding this two the total drag produced on the stationary particle can be found out.

$$F_D = -\int_0^\pi \tau_{r\theta}\sin\theta dA - \int_0^\pi \cos\theta dA \tag{3.3}$$

where, F_D= total fluid drag on the sphere, $dA(= 2\pi a^2 \sin\theta d\theta)$= surface integrand. For an unbounded flow the integral leads to [50]

$$F_D = 6\pi\mu\mathbf{u}a \tag{3.4}$$

which is the famous Stokes equation named under a pioneer fluid mechanist George Gabriel Stokes. It should be mentioned that, this formula is strictly valid for creeping flow or when Reynolds number $(Re) < 1$. The dimensionless number, Reynolds number(Re) specifies whether the flow in a channel is laminar or turbulent? Reynolds number is defined as,

$$Re = \frac{\rho v D}{\mu} \tag{3.5}$$

here, ρ = Fluid density, v = Fluid velocity, D = Diameter of channel, and μ = viscosity of fluid. For pipe flow if $Re \leq 2100$ the flow is considered laminar and if $Re \geq 2300$ the flow is assumed to be turbulent. For $Re < 1$ the flow is considered in stokes flow regime.

For the particle motion in a region bounded by channel wall the value of this drag force increases. This increased drag is usually characterized by two wall correction

factors. The first case considers a uniformly moving particle through a stationary fluid. In this case the ratio of the actual drag to the Stokes drag is termed as wall correction factor K_1. If the value of the actual drag force in this case is F_1, K_1 can be expressed as:

$$K_1 = \frac{F_1}{F_D} \tag{3.6}$$

which yields

$$F_1 = K_1 6\pi\mu \mathbf{u} a \tag{3.7}$$

The second case considers a stationary particle held fixed in a moving fluid. This wall correction factor is termed as K_2. In case of pressure driven flow the drag on the particle is calculated in terms of the maximum velocity v_{max} inside the channel. If the value of the actual drag force in this case is F_2, K_2 can be expressed as:

$$K_2 = \frac{F_2}{F_D} \tag{3.8}$$

that yields

$$F_2 = -K_2 6\pi\mu v_{max} a \tag{3.9}$$

The minus sign accounts for the fact that, in this case the direction of the force exerted by the flowing fluid on the particle is opposite to that found from the previous case.

3.2 Electric double layer (EDL)

Some organic (polystyrene, plexiglass) or inorganic polymers (glass) gain a surface electric charge if immersed in an electrolyte. The fixed charge can arise from dissociation of surface chemical groups of either the polymer substrate itself or of adsorbed additives. Counter ions present in the electrolyte are attracted to the charged solid surface due to the coulombic force and form an electric double layer(EDL). In the immediate proximity, the counter ions are tightly bound to the charged surface and thus become immobile. This thin part of EDL is called the Stern layer.Relatively away from the solid surface is the diffusive part of EDL, where the attraction coulombic force is relatively weak due to distance and the counter ions remain mobile. The diffusive layer is usually much wider than the Stern layer. The imaginary surface between the diffusive and the Stern layers is called the outer Helmholtz plane (OHP).The electric potential localized on this surface is an important characteristic of EDL, so-called zeta-potential(ζ) which is for simplicity usually considered as the wall potential.

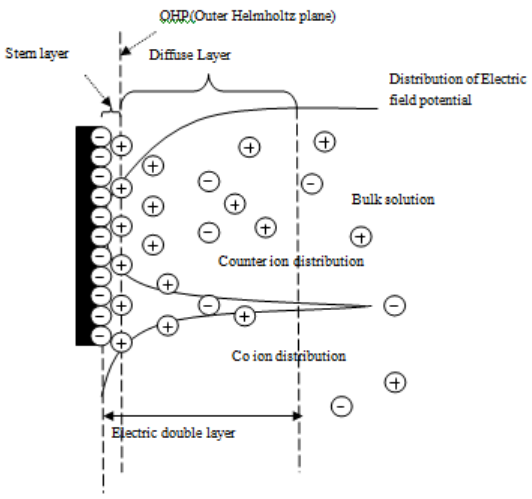

Figure 3.2: Electric double layer over a charged surface

The EDL structure, depicted in Fig 3.2 represents a typical equilibrium state that is established when: (a) the dielectric or the electrode surface is in contact with the electrolyte for a sufficient time, (b) any temperature changes and bulk concentration changes do not occur in space and time, and (c) the electrolyte does not move. These conditions are often not satisfied in real applications and thus the EDL structure can be more complex. The EDL width is approximately equal to the inverse Debye length κ^{-1}. For a symmetric uni-univalent electrolyte, the inverse Debye length can be estimated as [31],

$$\kappa^{-1} = \sqrt{\frac{2z^2e^2n_\infty}{\epsilon k_B T}} \tag{3.10}$$

where, k_B= Boltzmann constant, T= absolute temperature, ϵ= permittivity of fluid, z= valency of ion, e= fundamental charge, n_∞= bulk concentration of ion.

3.3 Relaxation of Electric Double Layer

As soon as a nonconducting/ dielectric sphere is immersed in an electrolyte, it will obtain a surface charge and an electric double layer starts to form around the particle. Within a very short time EDL forms completely and practically screens the electric field created by the charged sphere. The charge cloud around the sphere is completely symmetric and produces zero net force on the particle if sphere and the surrounding electrolyte is stationary or there is no external electric field. If there is a relative motion between the sphere and the surrounding electrolyte, the symmetry of the EDL will be disrupted (Fig 3.3) resulting a polarized EDL as well as a net electric field around the sphere. This electrokinetic phenomena is termed

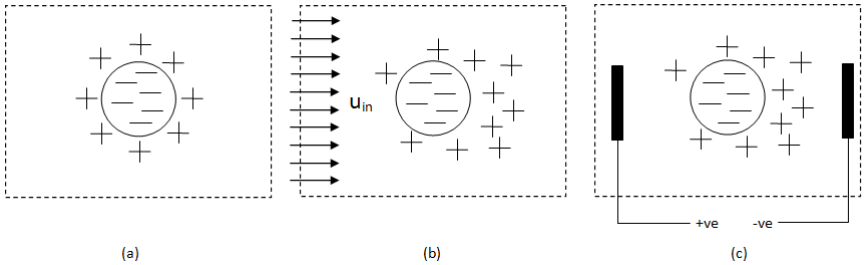

Figure 3.3: a) Uniform electric double layer around charged particle in absence of flow or electric field, Distortion of EDL caused by b) fluid flow, c) electric field

as "relaxation".

To get a more vivid picture of relaxation, consider a spherical particle containing a finite surface charge is immersed in a stationary electrolyte as shown in Fig 3.3. In absence of any relative motion between the particle and electrolyte or external electric field a symmetric EDL will be formed around it. But just when a flow is imposed, due to the finite size of the ions the flow will drag the counter ions of diffuse double layer to the downstream of the particle. This will result in a concentration gradient between the upstream and downstream of the particle as in Fig 3.3.After a certain period of time known as 'relaxation time' by convection, diffusion and migration the ions will produce a steady polarized electric double layer. More counter ion will be amassed at the downstream of the polarized EDL and will give rise to a local electric field. Now this electric field will interact with the charged sphere and produce a net electric force on the particle. Similar scenario will occur if an external electric field is applied instead of the flow.

3.4 Maxwell stress

A dielectric substance when placed in an electric field, causes its positive charges to displace toward the field and negative charges move to the opposite direction. This creates an internal electric field that reduces the overall field within the dielectric itself. Due to the presence of these polarized charge, a dielectric substance experiences a force when placed in an external electric field.

The Korteweigh-Helmholtz electric force per unit volume ($\mathbf{f}$)for an incompressible fluid (dielectric substance)is given as,

$$\mathbf{f} = \rho_f \mathbf{E} - \frac{1}{2} E^2 \nabla \epsilon \tag{3.11}$$

where, ρ_f= charge density, $\mathbf{E}$= electric field, ϵ=permittivity of the fluid.

The term $\rho_f \mathbf{E}$ represents the body force due to the interaction of free charge in the fluid with the electric field. The second term accounts for the inhomogeneity in the permittiviy of the medium. For a linear dielectric we know, electric displacement,$\mathbf{D} = \epsilon \mathbf{E}, \nabla \cdot \mathbf{D} = \rho_f$. Using these values Eq 3.11 can be written as,

$$\mathbf{f} = \nabla \cdot [\epsilon \mathbf{E}\mathbf{E} - \frac{1}{2}\epsilon \mathbf{E} \cdot \mathbf{E}\bar{I}] \tag{3.12}$$

The term inside the square bracket is referred as Maxwell stress tensor $\overline{T}$.Here $\bar{I}$ is an identity tensor of second order, defined as

$$\bar{I} = \begin{pmatrix} 1 & 0 & 0 \\ 0 & 1 & 0 \\ 0 & 0 & 1 \end{pmatrix}$$

The force arising from Maxwell stress tensor on a body of volume V enclosed by a surface S is given by

$$F = \int_V \mathbf{f} dV = \int_V (\nabla \cdot \overline{T}) dV$$

Using divergence theorem,

$$F = \int_V (\nabla \cdot \overline{T}) dV = \int_S (\mathbf{n} \cdot \overline{T}) dS$$

Utilizing the symmetry of Maxwell stress tensor, the above equation can be written as

$$F = \int_S (\overline{T} \cdot \mathbf{n}) dS$$

So the force acting on a dielectric in an electric field

$$F = \int_S [\epsilon \mathbf{E}\mathbf{E} - \frac{1}{2}\epsilon \mathbf{E} \cdot \mathbf{E}\bar{I}] \cdot \mathbf{n} dS \tag{3.13}$$

3.5 Model geometry

A finite length 3D circular cylindrical channel of lenght L and radius b with a single paraboloid shaped object protruded from the wall is considered as the problem geometry as shown in Fig: 3.4. The circular cylindrical channel is a simplification of flow vessel like micro and nano pore, blood vessel, microchannel etc. Length of the channel is considered to be sufficiently longer than the radius so that the

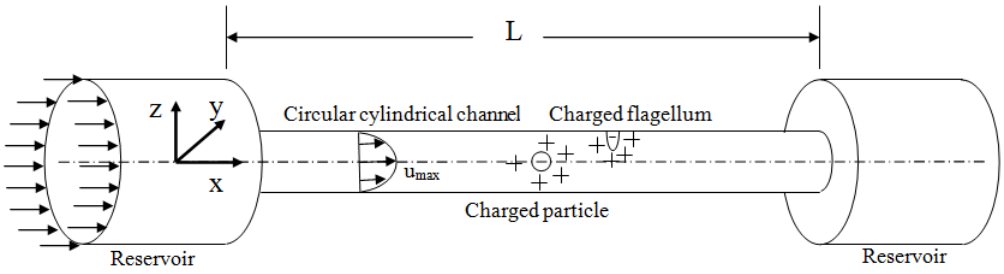

Figure 3.4: Problem geometry

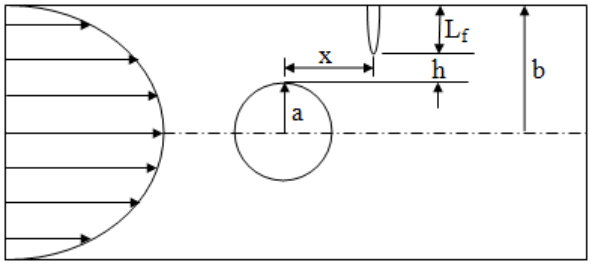

Figure 3.5: Different parameters in problem geometry

poiseuille flow gets sufficient time to develop fully. The finite length cylindrical channel terminates in two sufficiently large reservoirs at both end to eliminate any end effect. A paraboloid shape object protruded from the cylinder wall is assumed to represent any flagellum type object inside a flow channel. The length of the paraboloid is L_f with base radius r_f as shown in Fig:3.5.

A rigid particle of radius a is assumed to move along the centerline of the channel. The size of the particle is so chosen that its radius is equal to the flagellum length, $L_f = a$. A varying range of size ratio $\lambda = a/b$ has been considered to check the effect of size ratio but always a separation gap between particle and flagellum ($b-a-L_f > 0$) is maintained. Along with size ratio(λ) two more dimensionless parameters is conceived to study the problem. They are scaled axial distance between particle center and flagellum axis, $\alpha = x/b$ and scaled separation distance, $\beta = (b-a-L_f)/b$.

An mono-valent electrolyte solution of density ρ and viscosity μ is flown through the channel over the stationary particle by applying a pressure gradient across the channel. Presence of charge on the particle and flagellum establish an EDL over them which almost immediately distorted by the presence of the flow. Drag force on the particle caused by the flow field and electric field at different separation gap, axial distance, solute concentration and particle size ratio is of prime interest in this problem.

In this problem the typical channel diameter is assumed to be 20μ m which is equivalent to venule diameter. The typical particle size is considered to be around 8μ m that is the larger diameter of Erythrocyte (RBC). The flowing fluid is considered to be a mono-valent electrolyte dissolve in water having density of $1000Kg/m^3$ and viscosity 0.001 Pas. Fluid velocity for this kind of problem is of order 10^{-6} resulting in Reynolds number of order 10^{-5} which makes the flow strictly in creeping flow regime. The typical bulk concentration is assumed to be of order 10^{-10}.

3.6 Governing equations and associated boundary conditions

3.6.1 Applicability of Continuum Mechanics

A dimensional number known as Knudsen number (Kn) is used to determine whether Continuum Mechanics or Statistical Mechanics is applicable to address a problem. Knudsen number is defined as the ratio of molecular mean free path to a representative physical length scale, here the channel diameter. Mathematically,

$$Kn = \frac{\lambda_m}{D} \tag{3.14}$$

where, λ_m= Molecular mean free path in medium, D= Physical length scale. If Kn$\ll$1 Continuum Mechanics is applicable and if Kn is near unity Statistical Mechanics is appropriate choice.

For liquid water the mean free path is 2.5×10^{-10}m and in this problem the typical channel diameter is assumed to be20×10^{-6}m. This makes the Knudsen number to be 1.25×10^{-5} which is much less than unity. So for this particular problem at hand it is justified to use Continuum Mechanics.

3.6.2 Navier Stokes equation

The NavierStokes equation, named after Claude-Louis Navier and George Gabriel Stokes, describes the motion of fluid substances.This equations arises from applying Newton's second law to fluid motion, together with the assumption that the stress in the fluid is the sum of a diffusing viscous term (proportional to the gradient of velocity), a pressure term and a body force term - hence describing a viscous

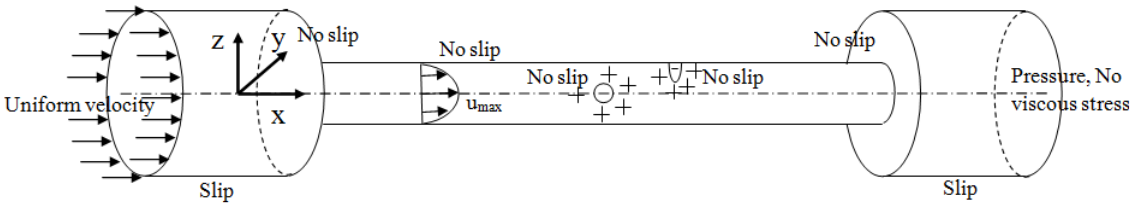

Figure 3.6: Boundary conditions for Navier Stokes equation

flow.The vector form of Navier-Stokes equation is [29]

$$\rho(\frac{\delta \mathbf{u}}{\delta t} + \mathbf{u} \cdot \nabla \mathbf{u}) = -\nabla p + \mu \nabla \cdot (\nabla \mathbf{u} + \nabla \mathbf{u}^T) + \mathbf{F}_b \tag{3.15}$$

where, $\mathbf{u}$= Fluid velocity, ρ= Fluid density, μ= Viscosity, p=Pressure,$\mathbf{F}_b$= Body force, t= time

Navier-Stokes equation has four unknown parameters (u_x, u_y, u_z and p) and three equations. As a result Navier-Stokes equation is always solved coupled with continuity equation,

$$\nabla \cdot \mathbf{u} = 0 \tag{3.16}$$

NavierStokes equations is a nonlinear partial differential equation in almost every real situation. In some cases, such as one-dimensional flow and Stokes flow (or creeping flow), the equation can be simplified to linear equation. The nonlinearity makes most problems difficult or impossible to solve analytically and is the main contributor to the turbulence. The nonlinearity is due to convective acceleration, which is an acceleration associated with the change in velocity over position.

In the present problem, it has been considered that the flow field is steady and hence the transient term is eliminated. Although the flow is creeping flow, the nonlinear term is considered during solution. The body force arises in the problem due to the electrostatic interaction between the point charges. The body force is calculated as

$$\mathbf{F}_b = \rho_f \mathbf{E}$$

$$\mathbf{F}_b = \sum_{i=1}^{n} (n_i z e)\mathbf{E}$$

$$\mathbf{F}_b = ze(n_p - n_n)\mathbf{E} \tag{3.17}$$

where, ρ_f= Space charge density, n_i= Concentration of i^{th} ion, z= Valency of ion, e= Elementary charge, $\mathbf{E}$= Electric field, n_p, n_n= Concentration of positive and negative ion

So the equation that dictates the flow field in the problem stands,

$$\rho(\mathbf{u}\cdot\nabla\mathbf{u}) = -\nabla p + \mu\nabla\cdot(\nabla\mathbf{u} + \nabla\mathbf{u}^T) + ze(n_p - n_n)\mathbf{E} \tag{3.18}$$

$$\nabla\cdot\mathbf{u} = 0 \tag{3.19}$$

To solve the equation using finite element method different plausible boundary conditions have to be assigned at different geometric boundaries. A uniform velocity boundary condition($u = U$) is considered at reservoir inlet and zero pressure and no viscous stress ($(\mu(\nabla u + (\nabla u)^T))\mathbf{n} = 0, p = 0$) at reservoir outlet. Experience shows that this performs better than assigning pressure at both ends. No slip ($u = 0$) condition is considered at channel wall, particle and flagellum surface. Slip boundary ($\mathbf{n}\cdot\mathbf{u} = 0, [-p\mathbf{I} + \mu(\nabla u + (\nabla u)^T)]\mathbf{n} = 0$) is assigned at reservoir wall to eliminate any kind of flow development inside the reservoir. All the boundary conditions are illustrated in Fig 3.6

3.6.3 Poisson equation

Presence of charge on the particle and flagellum surface and ions in solution set up an electric field inside the channel which eventually produces a force on the particle and flagellum and also affect the distribution of movable ions. The generated electric field distribution by Poisson equation which is stated as below

$$-\nabla^2\cdot\psi = \frac{\rho_f}{\varepsilon} \tag{3.20}$$

where, ψ= Electric potential, $\varepsilon(\varepsilon_0\varepsilon)$= Electrical permittivity of the medium i.e electrolyte solution
Replacing the space charge density ρ_f the equation can be rewritten as

$$-\nabla^2\cdot\psi = \frac{ze(n_p - n_n)}{\varepsilon} \tag{3.21}$$

In the present problem the only charged components are the particle and the flagellum. All the boundary conditions used in solving Poisson equation are illustrated in Fig: 3.7. The channel wall is considered uncharged assigning a zero surface charge ($-\mathbf{n}\cdot\mathbf{D} = \rho_f$) boundary condition. A constant surface charge density ($-\mathbf{n}\cdot\mathbf{D} = \rho_f$) is assigned at the surface of the particle and flagellum. The charge density is obtained by solving Poisson and Nernst-Plank equation in a separate model for an isolated particle assigning a surface potential (zeta potential), $\zeta = -1$ at the particle surface. From the solution the charge density is calculated and used in the

present model. Zero potential ($\psi = \psi_0$) is set at the inlet of left reservoir that acts as a reference potential for solving Poisson equation. Complexity arises while assigning boundary conditions for the reservoir wall and second reservoir outlet. There exist no well defined boundary condition for them. So it is assumed that they are sufficiently far away from the particle and flagellum that electric field component at those boundaries becomes zero. For the reason, a zero surface charge boundary condition ($-\mathbf{n} \cdot \mathbf{D} = \rho_f$) is set there [31].

3.6.4 Nernst-Planck equation

The NernstPlanck equation is conservation of charge equation used to describe the transport of chemical species in a fluid medium. It describes the flux of ions under the influence of both an ionic concentration gradient and an electric field. It extends Fick's law of diffusion for the case where the diffusing particles are also moved with respect to the fluid by electrostatic forces. The general form of Nernst-Planck equation is

$$\frac{\delta n_i}{\delta t} = -\nabla \cdot \mathbf{j} \tag{3.22}$$

$$\mathbf{j} = \mathbf{u} n_i - D(\nabla n_i - \frac{z e n_i}{k_B T} \nabla \psi)$$

where, j= flux of i^{th} ions, n_i= concentration of i^{th} ion, D= Diffusivity, k_B= Boltzmann constant, T= Absolute temperature

In the present problem, the advantage of using Nernst-Planck equation is that it can give a better insight in ion movement due to convection, diffusion and migration phenomena rather than just assuming Boltzmann distribution of ions around the charged bodies. For this reason, effect of relaxation and EDL overlap can be quantified properly. The present problem is considered to be in steady state and two types (positive and negative)ions are considered. The Nernst-Planck equation

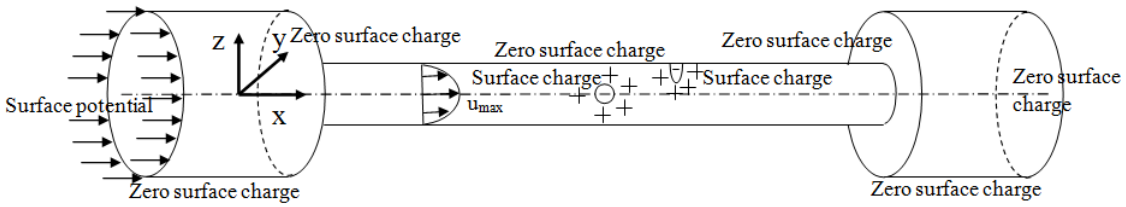

Figure 3.7: Boundary conditions for Poisson equation

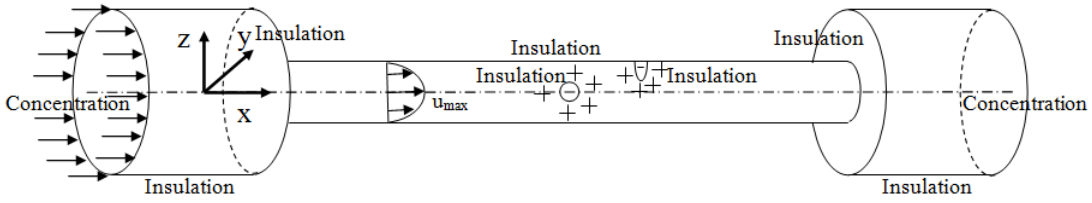

Figure 3.8: Boundary conditions for Nernst-Planck equation

used in developing the model for different species are

$$0 = \nabla \cdot (\mathbf{u}n_p - D(\nabla n_p - \frac{zen_p}{k_B T}\nabla\psi)) \tag{3.23}$$

$$0 = \nabla \cdot (\mathbf{u}n_n - D(\nabla n_n - \frac{zen_n}{k_B T}\nabla\psi)) \tag{3.24}$$

All the boundaries except the inlet and outlet of the reservoirs are set to be insulation/symmetry ($\mathbf{n} \cdot \mathbf{j} = 0, \mathbf{j} = \mathbf{u}n_i - D(\nabla n_i - \frac{zen_i}{k_B T}\nabla\psi)$. At reservoir inlet and outlet bulk concentration boundary condition ($n = n_0$) is assumed. All the boundary conditions are shown graphically in Fig: 3.8. This boundary is considered to be true as the reservoirs are far away from the charged particle and flagellum which makes the concentration at the reservoir same as bulk concentration. The drawback is that if there is any kind of salt rejection this model can not predict that. But since the charged surface is not long enough possibility of salt rejection or concentration polarization is very low [31].

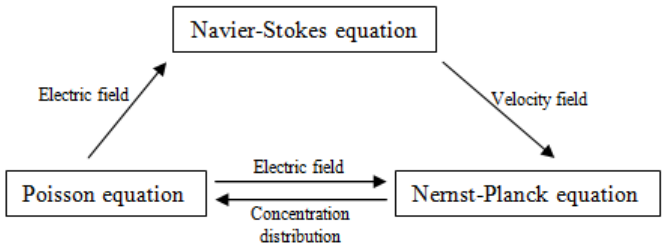

Figure 3.9: Coupling of governing equations

All the governing equations used in this model are coupled equation and need to be solved simultaneously. Poisson equation provides the electric field distribution but it takes the value of concentration of different species from Nernst-Planck equation. Navier-Stokes equation takes the electric field distribution to calculate the electrical body force on the fluid and gives the velocity field. Nernst-Planck equation using this velocity field along with the electric field from Poisson equation calculates the

Table 3.1: List of nondimensional parameters

Symbol	Dimensionless Parameters
$x^* = x/b$	x coordinate
$y^* = y/b$	y coordinate
$z^* = z/b$	z coordinate
$\alpha = x/b$	Axial distance of particle center and flagellum axis
$\beta = h/b$	Separation distance
$\kappa b = \kappa \cdot b$	Debye length
$\nabla^* = b \cdot \nabla$	Delta operator
$u^* = \frac{u}{(\frac{\varepsilon}{\mu b}(\frac{k_B T}{ze})^2)}$	Velocity
$p^* = p \cdot (\frac{b^2}{\varepsilon})(\frac{ze}{k_B T})^2$	Pressure
$\rho^* = \rho \cdot (\frac{\varepsilon}{\mu^2})(\frac{k_B T}{ze})^2$	Density
$\psi^* = \psi \cdot (\frac{ze}{k_B T})$	Potential
$E^* = E \cdot (\frac{zeb}{k_B T})$	Electric field
$D^*_{p/n} = D_{p/n} \cdot (\frac{\mu}{\varepsilon})(\frac{ze}{k_B T})^2$	Diffusivity
$n^*_p = n_p/n_0$	Positive ion concentration
$n^*_n = n_n/n_0$	Negative ion concentration
$q^* = q \cdot (\frac{zeb}{\varepsilon k_B T})$	Charge density
$F^* = \frac{Fa^3}{\epsilon}(\frac{ze}{K_B T})^2$	Drag force

concentration distribution, which it then provides to the Poisson equation. Fig: 3.9 shows the data flow graphically.

3.7 Nondimensionalization of governing equations

The discipline of fluid dynamics describes the motion of gases in extraterrestrial space, the dynamics of atmospheres and oceans,and the motion of blood in capillaries thinner than a human hair. To describe within a single framework events that span such a large range of time and length scales, fluid dynamics relies on a special mathematical entity 'Dimensionless Parameter'. All the parameters available in a problem are scaled using some scaling parameters. It brings all the parametric values in same or near order. The main advantage of using scaling parameters is that, it eliminates the presence of very large and very small parameter in the same problem which may cause computational error. To use this advantage all the governing equations are scaled or made dimensionless using some parameters enlisted in table 3.1.

Putting all these dimensionless parameters in the above governing equations the dimensionless governing equations stand,

Navier Stokes equation

$$\rho^*(\mathbf{u}^* \cdot \nabla^* \mathbf{u}^*) = -\nabla^* p^* + \nabla^* \cdot (\nabla^* \mathbf{u}^* + \nabla \mathbf{u}^{*T}) + \frac{1}{2}(\kappa b)^2 (n_p^* - n_n^*)\mathbf{E}^* \tag{3.25}$$

$$\nabla^* \cdot \mathbf{u}^* = 0 \tag{3.26}$$

Poisson equation

$$-\nabla^{*2} \cdot \psi^* = -\frac{1}{2}(\kappa b)^2 (n_p^* - n_n^*) \tag{3.27}$$

Nernst Planck equation

$$\nabla^* \cdot (n_p^* \mathbf{u}^* - D^* \nabla^* n_p^* - D^* n_p^* \nabla^* \psi^*) = 0 \tag{3.28}$$

$$\nabla^* \cdot (n_n^* \mathbf{u}^* - D^* \nabla^* n_n^* - D^* n_n^* \nabla^* \psi^*) = 0 \tag{3.29}$$

3.8 Finite Element Method (FEM)

Finite element method (FEM) is employed for solving the governing equations along with the boundary conditions in this study. The method is well described in literature [42] and is widely used for solving differential equations in many areas of engineering and science. In finite element method, a geometrically complex domain of the problem is discussed with simple elements. The elements are connected to each other at nodal points. The responses of the dependent variables are assumed a priori. State variables are approximated by basis functions, which are formulated from polynomials. Approximating piecewise function for state variables are known as test functions. Replacing the shape function in the discretized weak equations by the shape functions associated to each computational node gives a single algebraic equation which satisfies the discretized form of the governing equations. In this way a system of algebraic equations are formed. These equations describe the relationship between the coefficients of the test functions. Solving these algebraic equations for these coefficients the behavior of the dependent variable is obtained.

3.9 Implementation of model

A commercial finite element package Comsol Multiphysics has been used to solve couple Poisson, Nernst Planck, Navier-Stokes and continuity equations in steady state. Three dimensional geometry is considered in present problem which is then discretized using tetrahedral element. Higher number of mesh elements is used on near the flagellum and particle to facilitate capturing the higher electric field and/or

ion concentration gradient near the surface.
Intel Core i7 processor and 16 GB RAM are employed to obtain the solutions of present problem.

Chapter 4

RESULTS AND DISCUSSION

4.1 Model validation

A computational model of any problem must comply with the results available in literature for similar type of problems to ensure the accuracy of solution of the governing equations and boundary conditions, meshing and solution methodologies. For simplicity and accuracy the present model is validated against three different cases. The first case is purely hydrodynamic where a fluid is flowing over an uncharged stationary particle residing inside an uncharged pore. It is verified that whether the governing equations and boundary conditions can precisely predict the drag forces and drag coefficients. The second case verifies the ability of present model to predict the electrokinetic phenomena like electric field distribution, motion of charge etc. In the third case, the excess drag produces on a charged particle caused by the presence of charge on the particle is verified against published result. This ensures that all the coupling are done perfectly and the model is quite capable of evaluating the combined effect of hydrodynamics and electrokinetics. Verification using these three models are briefly discussed below.

4.1.1 Hydrodynamic drag of a particle

Values of drag factor (K_2) for the flow over a stationary uncharged sphere at the centerline of a cylindrical channel for different λ values are calculated by utilizing the present computation model which is a purely hydrodynamic model. These calculated values are compared with the published analytically and numerically computed results. Very accurate values of wall correction factors for all λ values were obtained as compared to singular perturbation techniques [9]. Values of wall correction factors were calculated by using spectral boundary element method, which

Table 4.1: Comparison of drag factor K_2

$\lambda = a/b$	Present computation	Quddus et al.[40]	Bungay-Brenner[9]	Higdon-Muldowney[25]
0.1	1.2305	1.2394	1.2548	1.2547
0.2	1.6205	1.6268	1.6345	1.6347
0.3	2.2148	2.2166	2.2285	2.2289
0.4	3.2046	3.2068	3.216	3.2157
0.5	4.9794	4.9837	4.9992	4.9953

further validated the previously provided results [25]. The latest investigation of this problem was done utilizing the Arbitrary Lagrangian Eulerian method [40]. In Table 4.1 the calculated values of drag factors K_2 from the present computation model is presented in tabular form, along with the values found from the above mentioned theoretical and numerical investigations. It is well noticeable that the values calculated by the present computation model are indistinguishable with the other results.

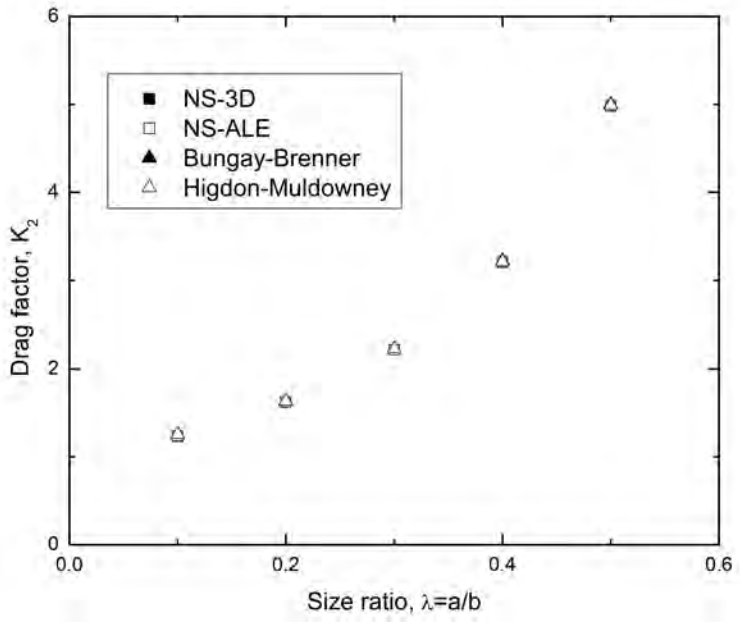

Figure 4.1: Comparison of drag factor (K_2) for centerline motion of particle

The percentage of error in K_2 for $\lambda = 0.1, 0.2, 0.3, 0.4, 0.5$ are $2.4\%, 0.87\%, 0.6\%, 0.34\% and 0.31\%$ respectively. The percentage of error is slightly high for $\lambda = 0.1$ and the drag factor is little under-predicted. The distortion of 3D mesh element near the particle for lower size ratio may be the reason behind it. A graphical comparison for the values of wall correction factor K_2 presented in Table is shown in Fig: 4.1.

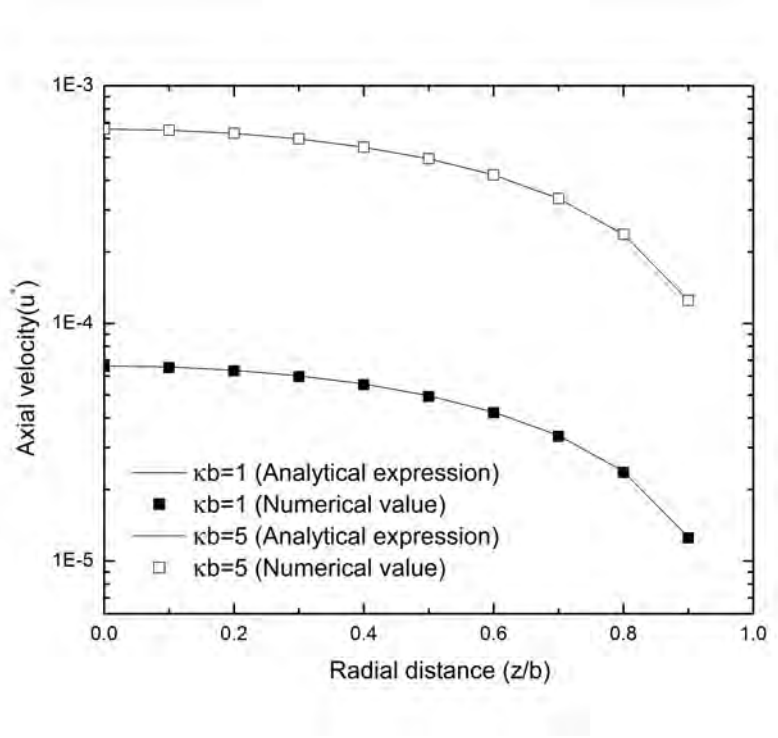

Figure 4.2: Comparison of velocity at different radial distance for different κa

4.1.2 Electrokineic flow velocity

Flow velocity of an electrolyte in presence of a charged wall under an applied pressure is calculated using present PNP-NS model. No particle is considered inside the channel. Applied pressure gradient(P_x) establishes a flow inside the channel that drag ions from the EDL and results in an electric field that oppose the flow. For varying concentration the flow velocity is at different radial distance is calculated and compared with the analytical values available in literature [31]. The flow velocity can be calculated from the following equation

$$u_x(r) = \frac{b^2 P_x}{4\mu}[1 - (\frac{r}{b})^2] - \frac{\varepsilon\psi_c}{\mu}[1 - \frac{I_0(\kappa r)}{I_0(\kappa b)}]\mathbf{E}_x \tag{4.1}$$

Comparison of analytical and numerical values calculated here is presented in Fig: 4.2. Both the values literally overlap each other.

4.1.3 Excess drag caused by presence of charge

Drag factor (K_2) is calculated for flow past a stationary,charged, spherical particle inside a channel. Due to the presence of charge, the drag force as well as the drag factor will be higher than the uncharged particle. This excess drag is calculated for (κb= 0.1)and compared with published result [14]. Two types of model (axisym-

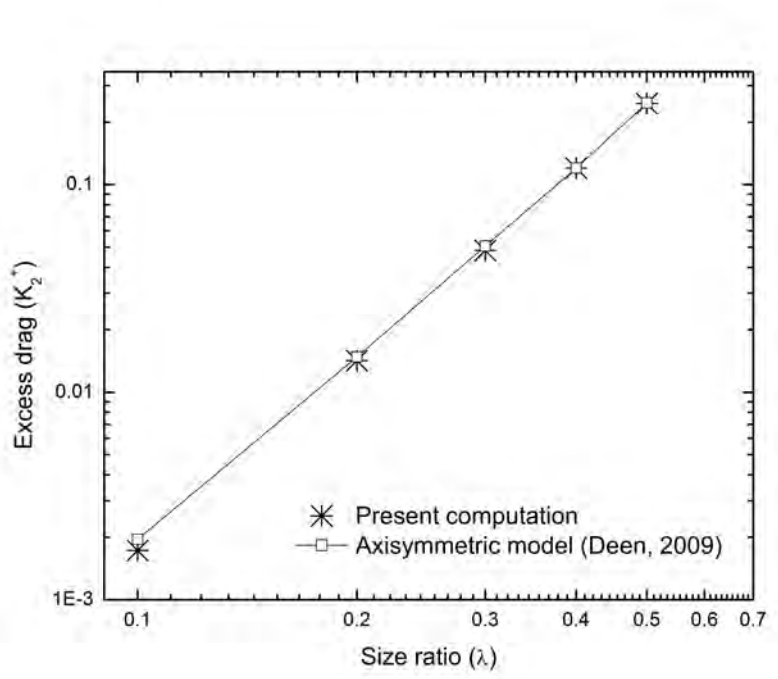

Figure 4.3: Excess drag caused by the presence of charge on particle for different size ratio at concentration, κb=0.1. Surface charge q^*=-5, u^*=0.45

metric and 3D models) have been developed to calculate the excess drag factor and compared with published result. Fig 4.3 illustrates the comparison. For concentration $\kappa b = 0.1$ excess drag calculated by both the axisymmetric and 3D model is very much similar to the published result ensuring the validity of developed model.

4.1.4 Mesh sensitivity analysis

FEM discretizes the whole computational domain into numerous small elements called mesh element and compute the dependent variables at the element node points. For any computational problem it is mandatory analyze whether the number of mesh element is sufficiently high to compute the dependent variables accurately at the nodes lying at complex geometry and where sharp changes occur. Here mesh sensitivity is analyzed to ensure proper meshing throughout the domain specially where the sharp change of fields occur, at the vicinity of sphere surface, region between particle and flagellum as example. Fig: 4.4 shows the discretization of the model.

Fig 4.5 shows the improvement of drag forces (hydrodynamic and electrical drag force) for different mesh number. A spherical particle of size ratio 0.5 is assumed

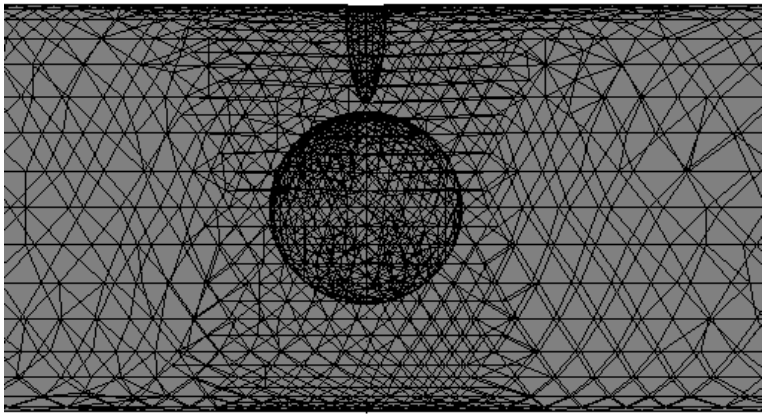

Figure 4.4: Discretization of problem geometry with adaptive mesh refinement near particle and flagellum

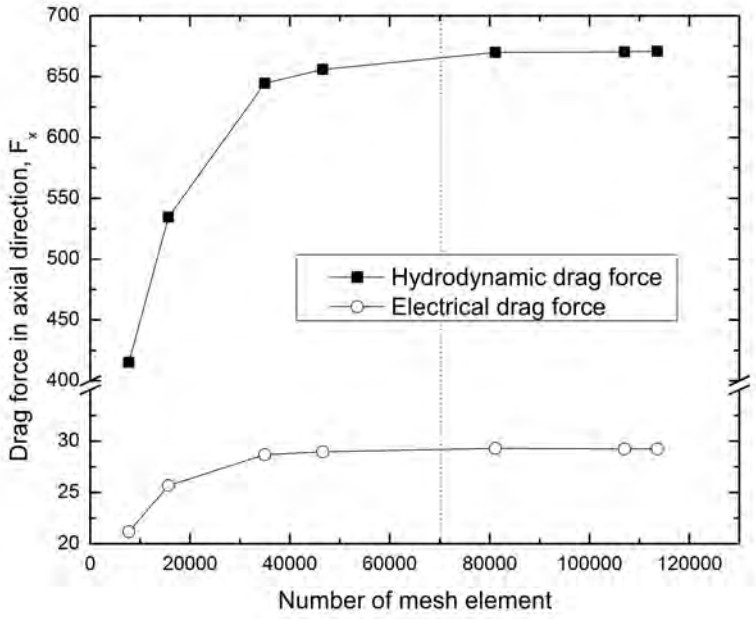

Figure 4.5: Hydrodynamic and electrical drag on particle for different mesh element, $\kappa b = 1$, λ=0.5, ψ^*=-1, u^*=0.45

to held stationary at the axis of a cylindrical channel while flow is past over it. The particle is carrying a surface charge of density q_s =-5 and the flowing fluid is assumed to be a electrolyte solution having concentration $\kappa b = 1$. The graph clearly shows after 80000 element the increment in both hydrodynamic and electrical drag is insignificant. It should be mentioned that, since the channel radius is considered as the length scale, changing λ will not affect the size of the computational domain but for smaller λ finer mesh element has to be created around the sphere. More over when the separation gap between the flagellum and sphere will be less dense mesh is needed around them to get correct result for concentration, potential and velocity field . Another important factor is that, for higher concentration ($\kappa b = 5$) dense mesh is mandatory around the particle and flagellum to track the sharp change in electric field. Keeping all these points in mind adaptive meshing is performed in this problem and approximately 120000 mesh element is used in every simulation to make them both accurate and time and memory efficient.

A good number of numerical model is solved throughout the study for clear understanding of the problem. A comprehensive summery of different models is tabulated in Table: 4.2 here for easy understanding of models in the upcoming sections.

4.2 Charged particle and flagellum interaction

4.2.1 Effect of separation gap between charged particle and flagellum

The effect of separation gap between charged particle and flagellum is quantified by the total drag force (or drag force only) on the particle in axial and lateral directions. The total drag force is the summation of both hydrodynamic drag force and electrical drag force on the particle. It must to be mentioned that, all the drag forces (total, hydrodynamic and electrical drag forces) are being scaled using appropriate scaling factor (Table: 3.1). Hydrodynamic drag force on the particle is caused by the finite viscosity of the flowing fluid and pressure gradient across the particle. On the other hand electrical drag force is produced due to a) electrostatic repulsion, b) relaxation of EDL, and c) EDL overlap. The separation gap is designated by $h = b - L_f - a$ as depicted in Fig: 4.6. For simplicity the length of the flagellum is assumed to be equal to the particle radius. Hence the size ratio ($\lambda = a/b$) which is defined as the ratio of particle to channel radius can be used to represent scaled separation distance ($\beta = 1 - 2\lambda$). Fig: 4.7 shows the variation of total drag force on

Table 4.2: Different models used in the study of present problem

Serial	Governing equations	Particle surface	Flagellum surface	Remarks
1	Navier-Stokes	Uncharged	Uncharged	Hydrodynamic drag force on the particle is obtained. No electrical body force
2	Navier-Stokes, Poisson, Nernst-Planck	Charged	Uncharged	Both hydrodynamic and electrical drag force is obtained. Electrical drag force is caused by charge relaxation around the particle caused by the flow. Presence of uncharged flagellum causes some EDL distortion in lateral direction resulting some relaxation drag force in lateral direction. Subtracting hydrodynamic drag force(1) from hydrodynamic drag force(2) will give the electrical body force caused by charge relaxation
3	Poisson, Nernst-Planck	Charged	Charged	Electrical drag force caused by electrostatic repulsion between particle and flagellum and undisturbed EDL overlap is obtained. The minute distortion in EDL is occurred by the presence of charged flagellum.
4	Navier-Stokes, Poisson, Nernst-Planck	Charged	Charged	Both hydrodynamic and electrical drag force is obtained. Electrical drag force is caused by charge relaxation around the particle caused by the flow, electrostatic repulsion and EDL overlap. Subtracting electrical drag force (2) and (3) from electrical drag force (4) will give the electrical drag force caused by distortion of overlapped EDL around the particle. Subtracting hydrodynamic drag force (2) form hydrodynamic drag force (4) will give the electrical body force caused by distorted and overlapped EDL.
5	Navier-Stokes, Poisson, Nernst-Planck	Charged	Oppositely charged	Both hydrodynamic and electrical drag force is obtained. Electrical drag force is caused by charge relaxation around the particle caused by the flow, electrostatic attraction and EDL overlap.

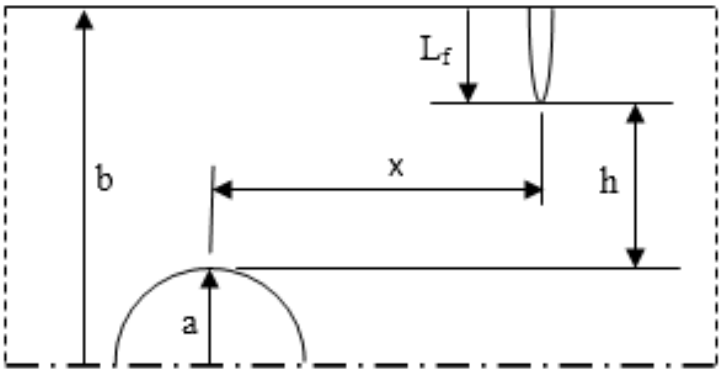

Figure 4.6: Separation distance and axial distance

the particle in axial direction for different β respectively. The particle is supposed to travel along the centerline of the channel and drag force is plotted at different axial distance ($\alpha = x/b$) between the flagellum and particle center.

Fig: 4.7 clearly shows that with the decrease of separation distance (β) or increase of size ratio (λ)the axial drag on the particle increases. It can be easily understood since with increase of particle size the local fluid velocity around the particle increases to keep the flow rate constant for every case. This increases the viscous drag on the particle. Along with this due to tightly fitted particle pressure drag also increases. Both of them increase the total hydrodynamic drag on the particle. This graph also shows that the drag is nearly uniform at the upstream and downstream of the flagellum but increases in the vicinity of the flagellum. But the interesting thing is that the position from where the particle starts to feel the presence of the flagellum is independent of size ratio or separation gap. For each λ the particle starts to feel the presence of the flagellum approximately in the range of $-1 < \alpha < 1$. The slender shape of the flagellum is predicted to be the reason behind the independence on the size ration or separation gap.

Fig 4.8 shows the percent increase in the axial drag for different separation distance. The increase is calculated while the particle center is just at the axis of the flagellum a place where the drag is maximum. This graph suggests that the increase in axial drag force is little sensitive to separation gap. The percent increase rages from 3.6% to 4.1% for separation distance 0.3 to 0.05. Fig: 4.9 shows the contribution of hydrodynamic drag force and electrical drag force to total drag force in axial direction. The graphs clearly shows in axial direction hydrodynamic drag force is the main contributor to total drag force providing 98.25% of it. The rest 2.75% is contributed by the electrical drag force.

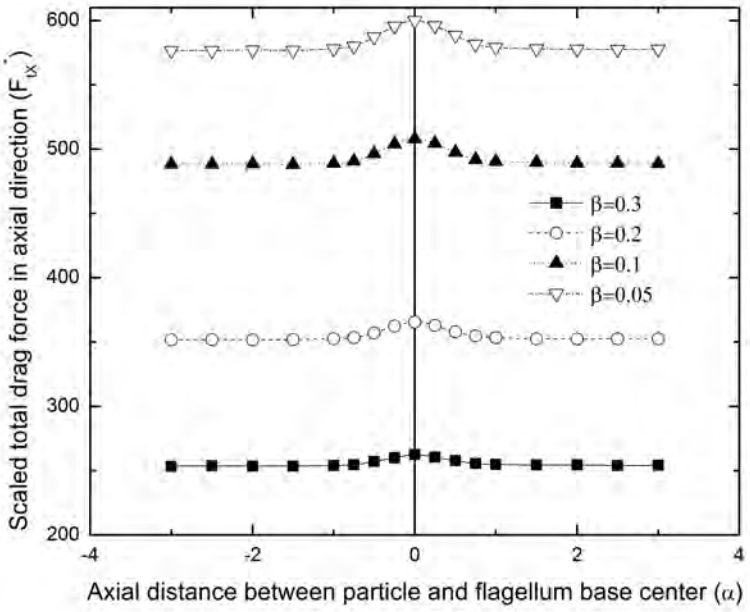

Figure 4.7: Scaled total drag force in axial direction for different separation distance (β) at different axial distance between particle center and flagellum axis(α), Particle and flagellum potential,ψ^* = -1, inlet velocity u^*=0.45

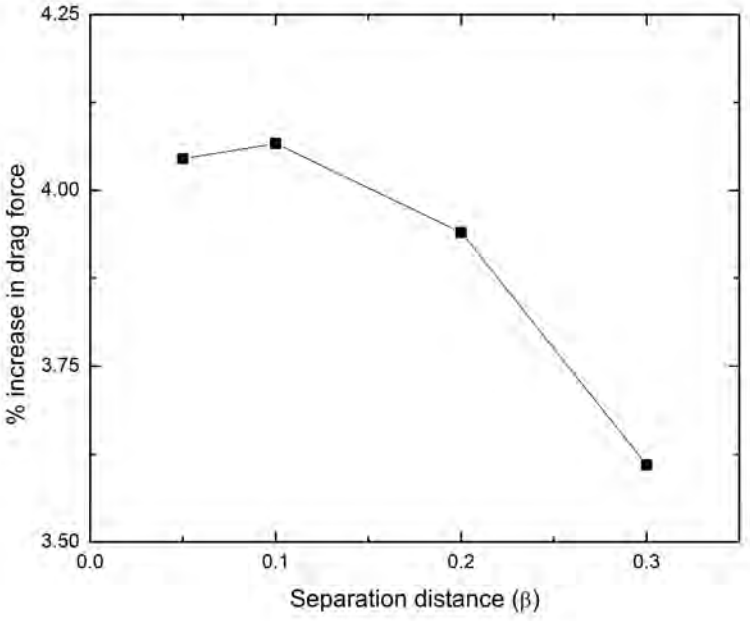

Figure 4.8: Percent increase in total axial drag vs separation distance (β)

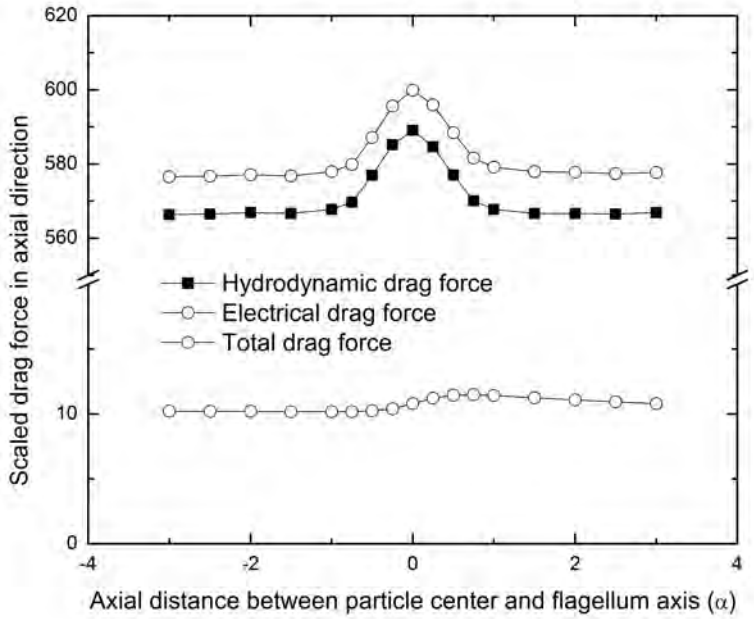

Figure 4.9: Components of scaled total drag force in axial direction, β=0.05, λ=0.475, ψ^*=-1, u^*=0.45

Fig: 4.10 shows the variation of drag force in lateral direction at different axial distance (α) at different separation distance (β).With the increase of size ratio (λ)or decrease of separation distance (β)total drag force in lateral direction increases. This drag force on the particle is summation of two forces electrostatic repulsion between the like charged particle and flagellum that always works in '-'ve z direction, and hydrodynamic drag force due to the motion of fluid. The net force acts in '-'ve z direction (displace the particle from channel centerline) when the particle is at flagellum upstream and in '+'ve z direction (bring back the particle to channel centerline) in downstream of the flagellum. Careful observation of the values suggests that drag force at upstream that tends to make the particle off centered is somewhat higher than the drag force at flagellum downstream that tries to restore the centerline position. For separation gap, β=0.3, 0.2, 0.1, and 0.05 the value of lateral drag at flagellum downstream is $11.92\%, 10.45\%, 8.55\%$, and 10.26% less respectively. Presence of charge on the flagellum and particle result in electrostatic repulsion which is the reason behind it. Fig: 4.11 shows the contribution of hydrodynamic drag force and electrical drag force to total drag force in lateral direction. The contribution of electrical drag force is near zero throughout the channel except the vicinity of flagellum where it becomes the main contributor contributing 83.91% at α=0. The contribution is nearly symmetric at flagellum upstream and downstream

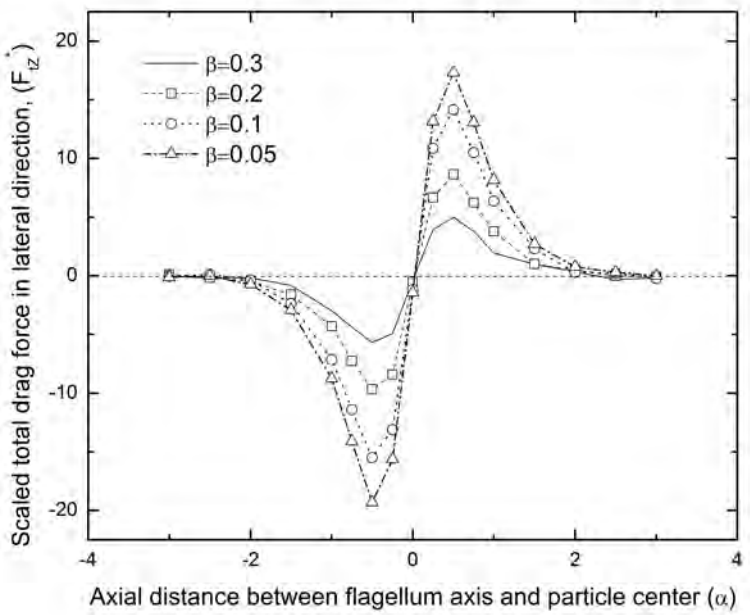

Figure 4.10: Scaled total drag force in lateral direction for different separation distance (β) at different axial distance between particle center and flagellum axis (α), Particle and flagellum potential,ψ^* = -1, inlet velocity u^*=0.45

but in opposite direction.

The variation of electrical drag force in axial and lateral direction for different size ratio (λ) or separation distance (β) is plotted against the axial distance between the particle center and flagellum axis (α)in Fig: 4.12 and Fig: 4.13 respectively. With the decrease of β electrical drag in both axial and lateral directions increase though the variation in lateral direction is little traceable. With the decrease of β the proximity of flagellum and particle increases that causes the drag force to increase. The graph also suggests that the nature of electrical drag force in lateral direction is symmetric in nature but axial electrical drag force is higher in flagellum downstream than the upstream. The behavior of electrical drag force is basically due to the distribution of charge around the particle and flagellum. Both of them produce EDL around them, that is been distorted by the flow. Additionally when the separation distance is low both EDL overlap. All these affect the ion distribution around the particle. Fig: 4.14 shows the negative ion distribution around the particle and flagellum for different separation distance.

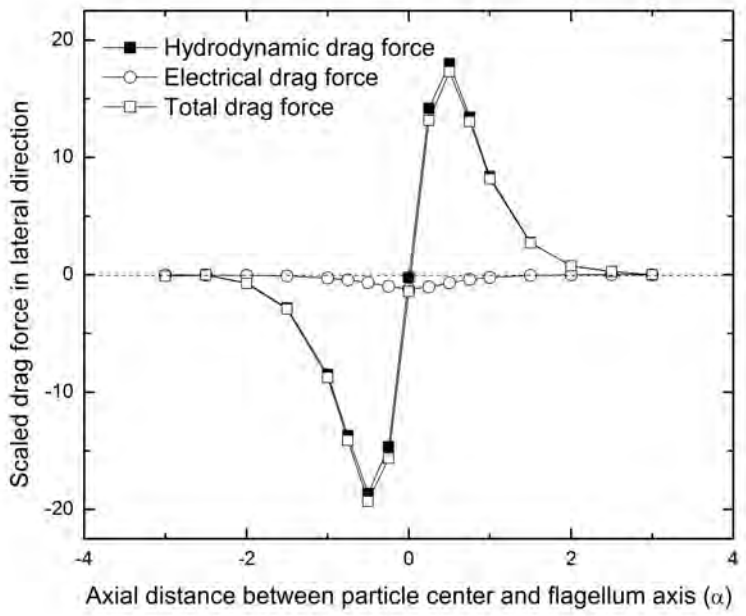

Figure 4.11: Components of scaled total drag force in lateral direction, β=0.05, λ=0.475, ψ^*=-1, u^*=0.45

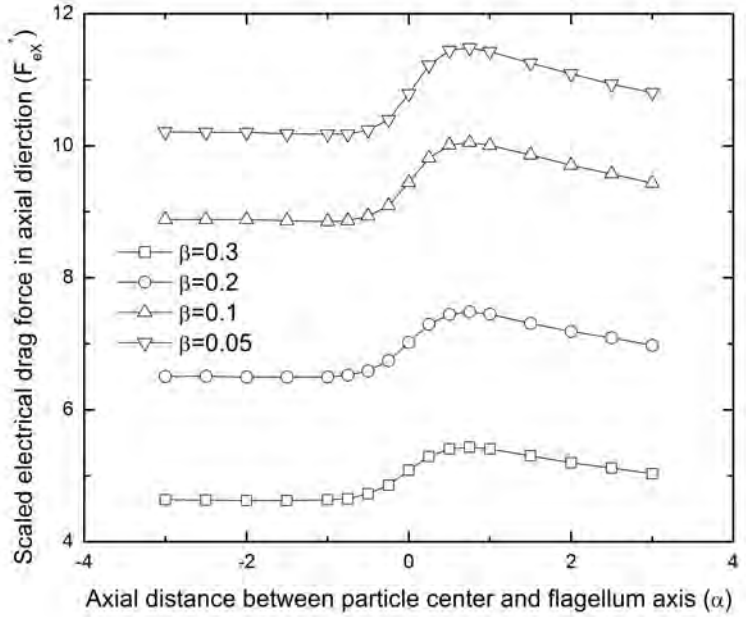

Figure 4.12: Scaled electrical drag force in axial direction for different separation distance (β) at different axial distance between particle center and flagellum axis (α), Particle and flagellum potential,ψ^* = -1, inlet velocity, u^*=0.45

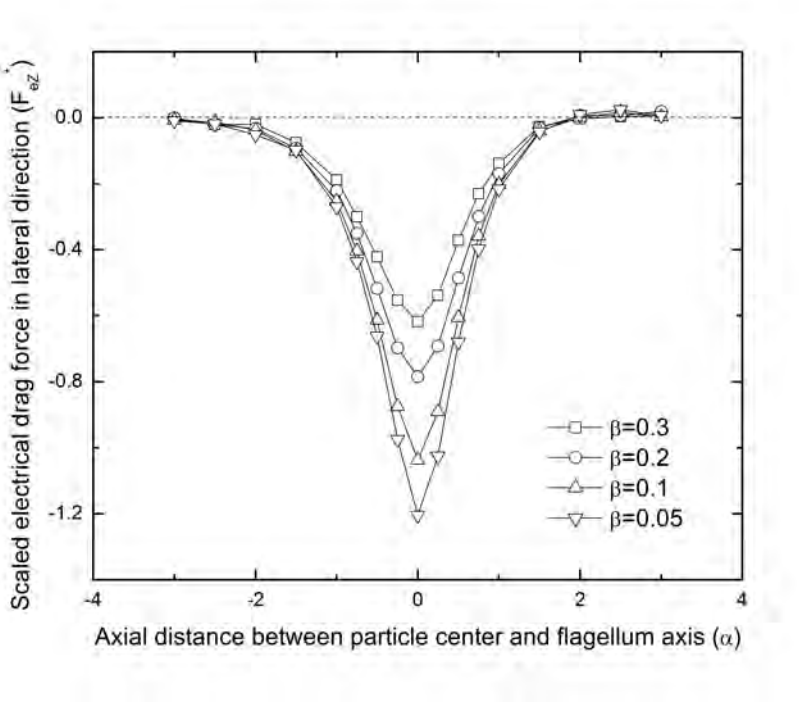

Figure 4.13: Scaled electrical drag force in lateral direction for different separation distance (β) at different axial distance between particle center and flagellum axis (α), Particle and flagellum potential,ψ^* = -1, inlet velocity, u^*=0.45

4.2.2 Consequence of charge presence in particle and flagellum

To understand the charge effect caused by the presence of like charge on particle and flagellum two different models are considered, a) flow over uncharged flagellum and uncharged particle and b) flow over charged flagellum and charged particle. For both the model the separation distance is considered to be 0.05. This choice is logical since previous results showed at this separation distance the effect is maximum. Total drag force in axial direction for both the model is plotted against axial distance of particle center form flagellum axis, α. in Fig 4.15. It shows that axial drag force is considerably higher for charged particle and flagellum than that of uncharged one. This suggests a stationary charged particle will feel more force in the flow direction than an uncharged one. So it is evident that surface charge plays a vital role in axial drag. Fig 4.16 shows the drag force in lateral direction at different axial distance of particle center form flagellum axis, α. Though barely distinguishable in Fig 4.16 percentage increase in drag force is higher for lateral direction in both upstream and downstream of flagellum than axial drag. The increase in axial drag force is somewhat constant but it varies in lateral direction. The interesting fact is that,

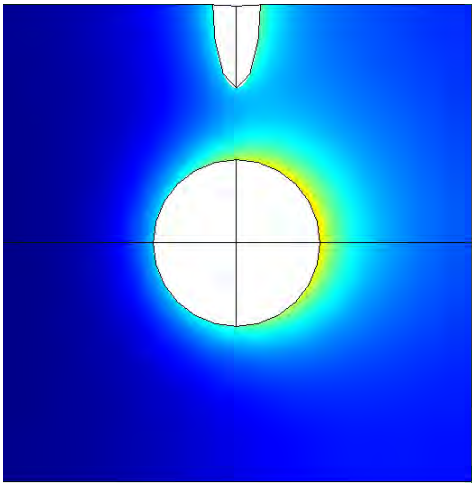

(a) Separation distance, β =0.3, λ=0.35

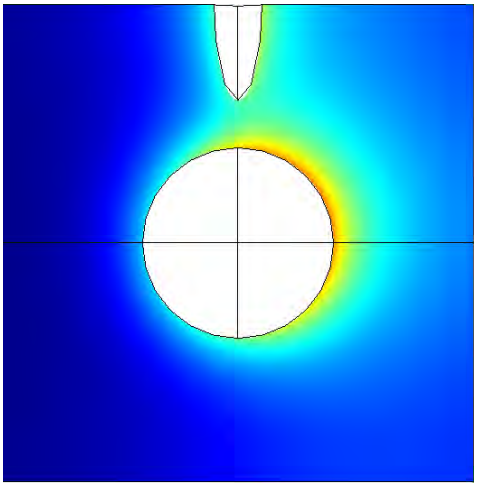

(b) Separation distance, β =0.2, λ=0.4

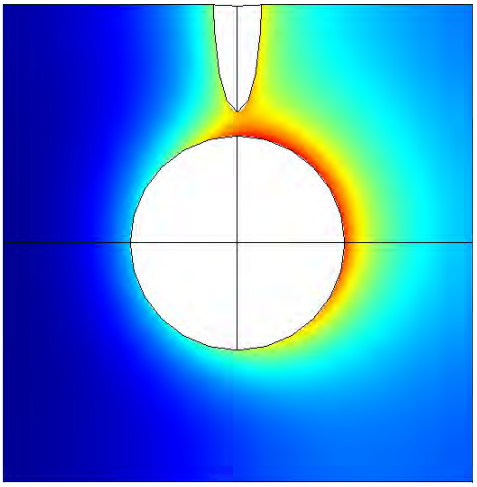

(c) Separation distance, β =0.1, λ=0.45

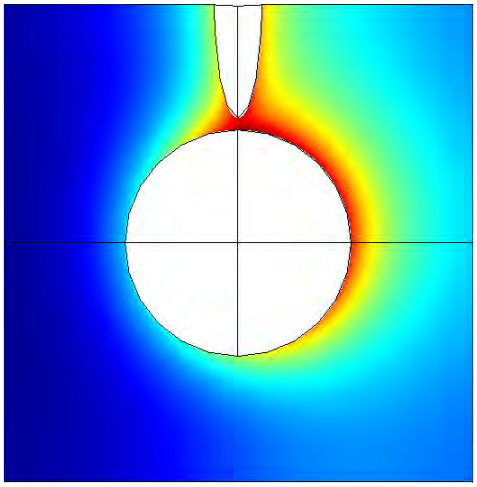

(d) Separation distance, β =0.05, λ=0.475

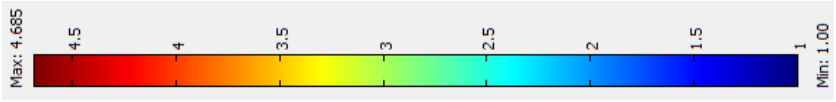

(e) Scale for color plot of scaled positive ion distribution around the particles and flagellum

Figure 4.14: Scaled positive ion distribution around the particle and flagellum for different separation distance at solution concentration κb=1

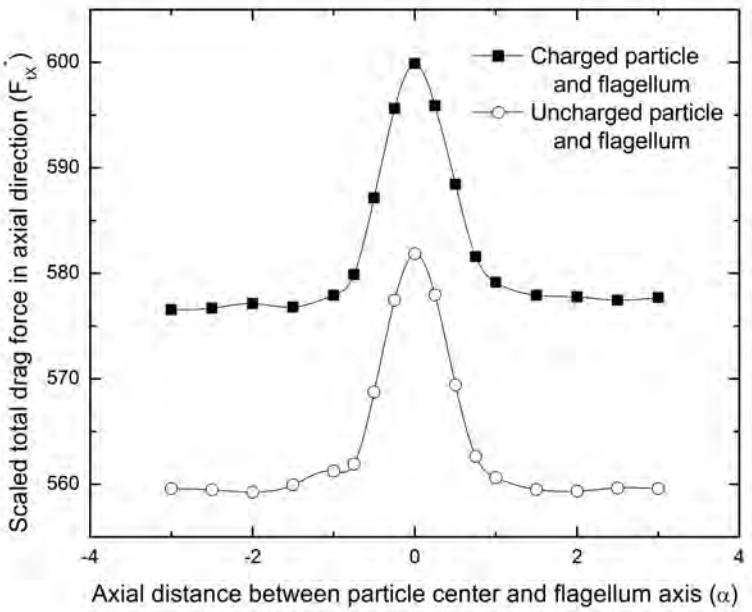

Figure 4.15: Scaled total axial drag force on particle at different axial distance between particle center and flagellum axis.Separation distance β=0.05, Particle and flagellum potential, ψ^* = -1 (charged condition), inlet velocity u^*=0.45

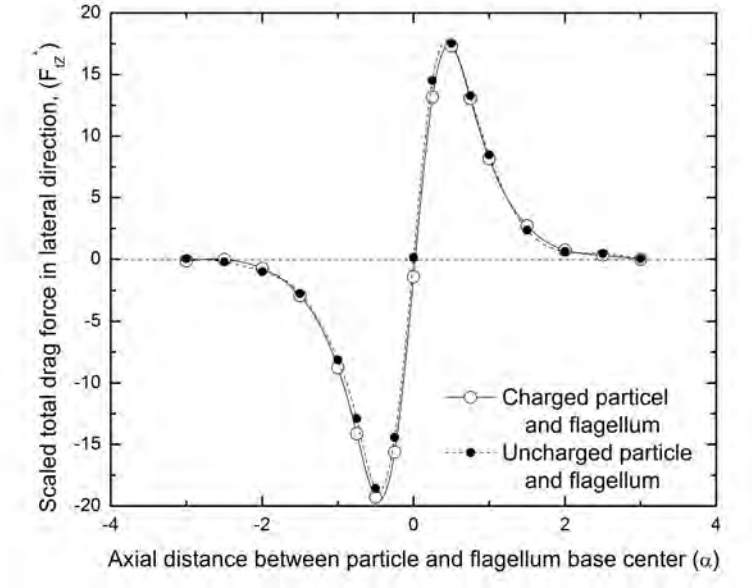

Figure 4.16: Scaled total lateral drag force on particle at different axial distance between particle center and flagellum axis.Separation distance β=0.05, Particle and flagellum potential, ψ^* = -1 (charged condition), inlet velocity u^*=0.45

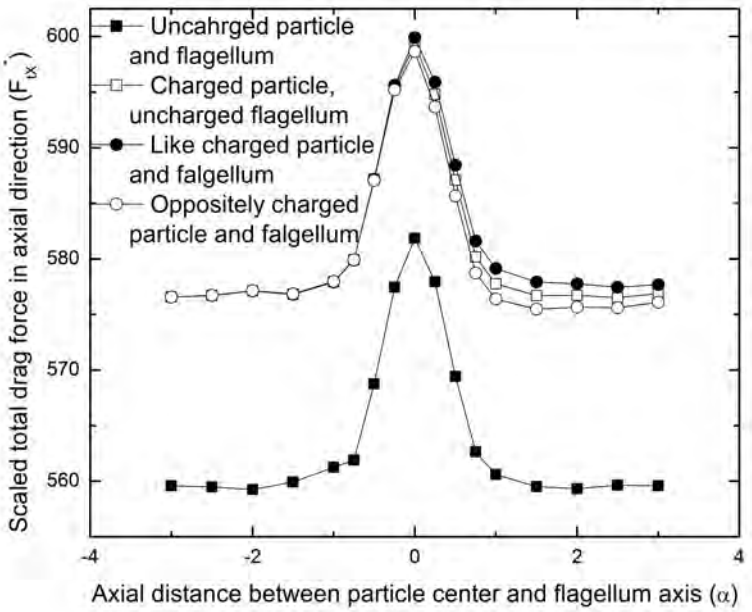

Figure 4.17: Scaled total axial drag force on particle at different axial distance between particle center and flagellum axis (for various charge condition on particle and flagellum). Separation distance β=0.05, Particle potential, ψ^*=-1 and flagellum potential, ψ^* = 1,-1, inlet velocity u^*=0.45

for an uncharged particle and flagellum, flagellum tends to move the particle from the center at its upstream and then brings it back with equal force. But in charged case, gives more force than uncharged case to make the particle off-centered and less force to bring it back. So for charged particle and flagellum particle the time taken to come back at channel center at downstream of flagellum will be more.

So far the effect of like charge on particle and flagellum is discussed. But there are still two more possible scenarios which are important from the context of present problem. One is uncharged flagellum and charged particle while the other one is particle and flagellum of opposite charge.

Fig 4.17 illustrates the effect of different charge conditions of flagellum on axial drag. Obviously for charged particle the axial drag is higher than uncharged one, but the interesting thing that the figure suggests, it is nearly independent of the charge condition of flagellum. Whatever the charge condition is on the flagellum (positive, negative or uncharged)axial drag at flagellum upstream is nearly insensitive to it. But at flagellum downstream the scenario is a bit different though the difference is too low. At downstream for particle and flagellum of like charge electrostatic

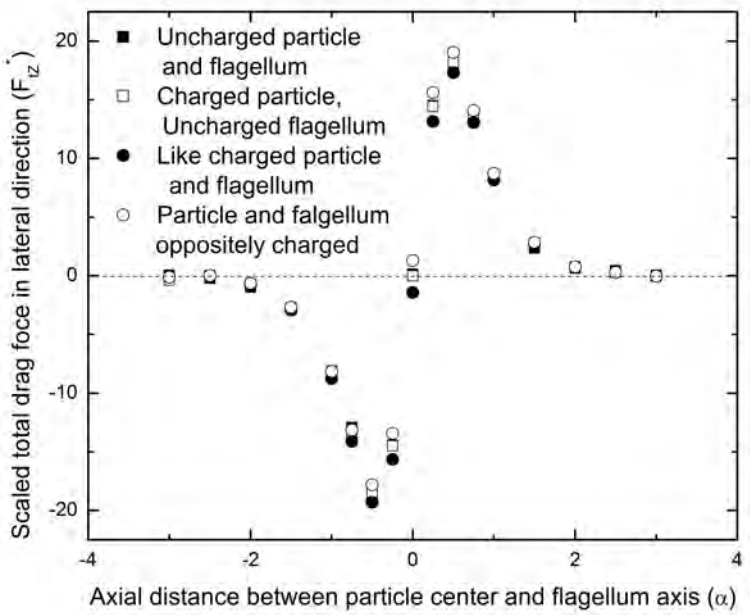

Figure 4.18: Scaled total lateral drag force on particle at different axial distance between particle center and flagellum axis (for various charge condition on particle and flagellum). Separation distance, β=0.05, Particle potential, ψ^*=-1 and flagellum potential, ψ^* = 1,-1, inlet velocity u^*=0.45

repulsion force acts in the direction of hydrodynamic drag force and increase the total drag force while for oppositely charged particle and flagellum electrostatic attraction force acts in opposite to hydrodynamic drag force and decreases the total drag force on the particle. For uncharged flagellum the total drag force is in-between.

Fig 4.18 illustrates the variation of lateral drag force on particle for different charge conditions (positive, negative or uncharged)of flagellum keeping the particle negatively charged. As previous, for like charged particle and flagellum the lateral drag force is higher at flagellum upstream and lower at flagellum downstream than that of oppositely charged flagellum and for uncharged flagellum the force is in-between.

4.2.3 Effect of relaxation

The presence of charge on particle and flagellum surface will affect the drag in three different ways, a) electrostatic repulsion and b) charge relaxation, and c) EDL overlap. Electrostatic repulsion is a fundamental phenomena that will always try to keep the charged particle away from the charged falgellum. As a result, at flagellum upstream it will act against the flow direction resulting in decrease of total drag

force and at flagellum downstream it acts in the same direction of flow and increase total drag force. Relaxation comes into play due to the distortion of EDL caused by the fluid flowing over the particle. Relaxation results in a concentration gradient across the particle that produces local electric field around the particle and affect the drag force on it. Fig 4.14 visually shows the relaxation effect i.e. concentration polarization around the particle. The reddish zone at the right of the particle shows the concentration of positive ion is greatly higher than left side. This will eventually give rise to an electric field and produce an electrical drag force.

To understand how the relaxation will affect the drag force the model of charged particle and uncharged flagellum is considered. Since the flagellum is uncharged the effect of electrostatic repulsion and EDL overlap are eliminated. So the only electrical drag obtained will be caused by relaxation. Another model solving the coupled Poisson and Nernst-Planck equation for charged particle and flagellum is used to calculate the combination of electrostatic repulsion force and EDL overlap wihout relaxation between then. Fig 4.19 shows the variation of electrical drag force in axial direction caused by electrostatic repulsion, relaxation and EDL overlap individually. It is evident from Fig 4.19, electrostatic repulsion and EDL overlap combinedly produce negative drag force at upstream and positive drag at flagellum downstream. But the drag produced by relaxation is relatively larger than repulsion effect and positive in nature hence eliminates repulsion effect in total drag force at both upstream and downstream. As a result, electrical drag force always increases the total drag force on the particle. Though seems to be uniform, relaxation effect decreases as the particle moves to the downstream of the flagellum. Disturbance in flow pattern due to the flagellum may be the reason behind it.But the effect is so small that it could be neglected. It should be noted that the plot showing the contribution of electrostatic repulsion and EDL overlap to axial electrical drag force in Fig: 4.19 is for undisturbed EDL while in real problem EDL is distorted due to fluid flow. As a result if we just simply add the two plot for relaxation and electrostatic repulsion + EDL overlap, the plot for the total electrical drag force for the present problem will not be obtained properly. Actually there is no possible way to separate all the contributors. The plot for axial electrical drag force for the present problem tells that at flagellum upstream the electrical drag is almost similar to drag force produced by relaxation (Fig: 4.19) only while the flagellum is uncharged, leaving any affect of repulsion. But what really happens is, fluid flow causes to accumulate more positive ion at the front of particle (relaxation), at the same time negatively charged flagellum draws more positive ion at the front of

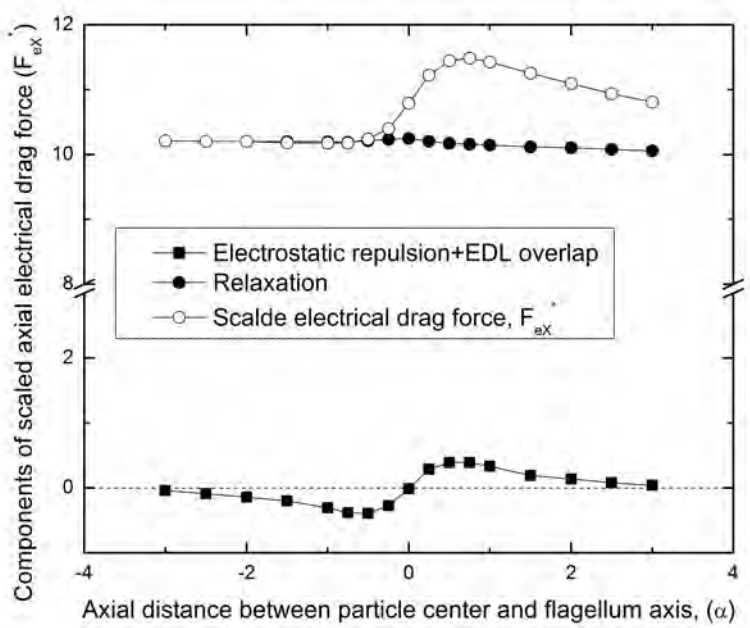

Figure 4.19: Contribution of different electrokinetic phenomena on scaled total electrical drag force in axial direction

particle. This extra ions produce more drag force and nullify the repulsion effect. The near the particle comes to flagellum the more the extra ion and the more the drag force. At flagellum down stream the distorted double layer around flagellum and particle overlaps and increases the electrical drag force rapidly.

The contribution of relaxation, electrostatic repulsion with undisturbed EDL overlap to lateral electrical drag is depicted in Fig 4.20. It clearly shows, in lateral direction electrostatic repulsion is the main contributor and relaxation is less effective in lateral direction. Since flow is assumed to take place in axial direction, so the deformation of EDL is expected not to happen in lateral direction resulting in smaller contribution of relaxation in lateral direction. To get a more vivid picture of the affect of relaxation Fig 4.21 shows the difference of concentration at four different points A, B, c and D. It clearly shows that concentration gradient between B and D is quite high and nearly constant throughout the whole axial distance. This results in near constant drag in axial direction. In lateral direction concentration gradient between A and C produces near the flagellum and drag force appears. The reason behind this accumulation of more positive charge at A is the disturbance in flow caused by the flagellum. Presence of particle inside the cylinder interrupts the flow and to keep the flow rate constant local fluid velocity around the particle increases.

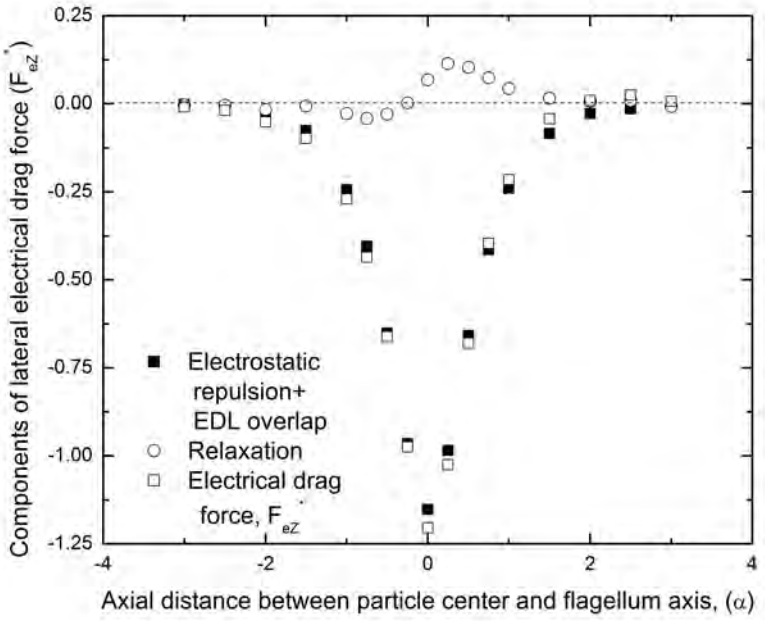

Figure 4.20: Contribution of different electrokinetic phenomena on scaled total electrical drag force in lateral direction

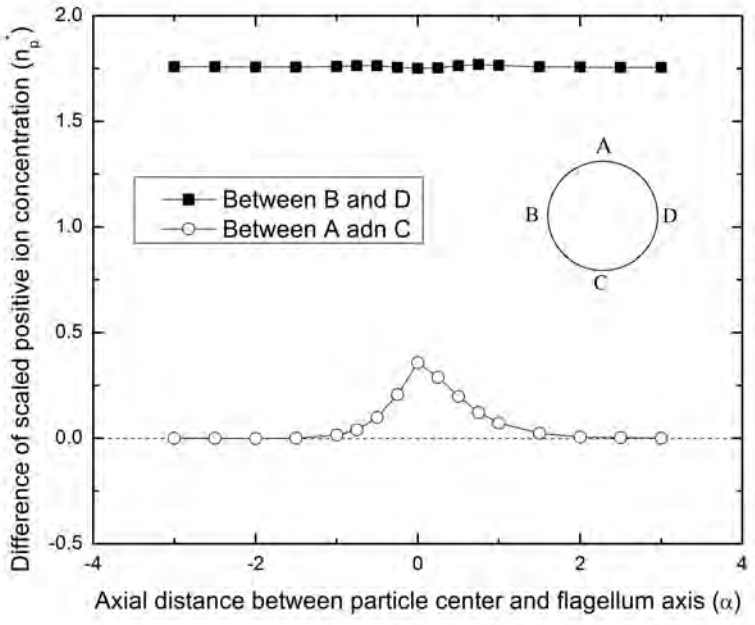

Figure 4.21: Concentration gradient at different points around the charged particle (ψ^* = -1) at different axial distance between the particle center and uncharged flagellum axis, u^*=0.45

But the presence of flagellum further disturb the flow and reduce it at the top of the particle. As a result the relatively high velocity flow at the bottom of the flagellum slightly moves in upward direction and drag more positive ion at the top of the particle.

4.2.4 Effect of EDL overlap

When the charged particle and charged flagellum come close to each other, their double layers overlap. At the same time both EDL distorted due to fluid flow. Nernst-Plank equation used in this model can address this complex distribution of ion caused by combined influence of convection, diffusion and migration. EDL overlap increases the concentration in the overlapped zone around the particle and affect the drag. This affect is quite visible in Fig 4.19 and Fig 4.20. In both figures, it is evident that electrical drag force for the present problem is neither similar to drag force caused by relaxation of a charged particle only nor the drag force caused by electrostatic repulsion and undisturbed EDL overlap, nor their summation. Distorted EDL overlap is the reason behind this difference. In both axial and lateral directions EDL overlap drag emerges at the vicinity of flagellum and starts to diminish at downstream. In axial direction EDL overlap drag force acts in the same direction of relaxation drag force and increase the total drag force. Fig 4.22 shows the concentration gradient between A, C and B, D for complete model of present problem and relaxation model (uncharged flagellum and charged particle model). The difference between two lines gives the effect of EDL overlap and electrostatic interaction on concentration distribution. Due to EDL overlap positive ion concentration at A and D increase rapidly, especially there is a leap at the concentration gradient between A and C. The proximity of flagellum tip and point A may be the reason and hence A experiences the maximum EDL overlap. It is easily understandable that, due to EDL overlap concentration gradient between B and D increases and total electrical drag force in axial direction increases. But although EDL overlap dramatically increases the concentration gradient between A and C but repulsion becomes so high that the total force act at -ve z direction.

4.3 Effect of concentration

The drag force acting on a charged particle confined in an uncharged cylindrical channel having flagellum like charged surface irregularity is the summation of hydrodynamic drag force and electrical drag force. Here electrical drag force has three components as discussed previously a)electrostatic repulsion, b) charge relaxation,

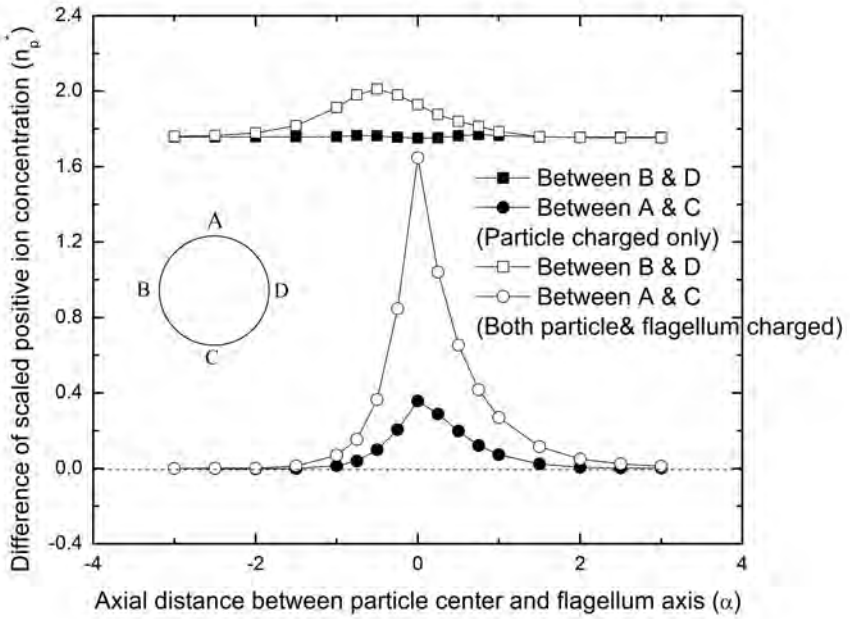

Figure 4.22: Concentration gradient at different points around the charged particle at different axial distance between the particle and flagellum base center (β=0.05, ψ^*= -1)

and c) EDL overlap. Both the charged particle and flagellum produce a symmetric electric double layer around them and the fluid flow distorted that symmetry and causes relaxation of EDL. While the particle and flagellum come close to each other their EDL overlap resulting in higher concentration in overlapped zone. One thing in common to both of these effects is that they both are dependent on the thickness of double layer which is expressed by inverse Debye length. Debye length is dependent of the concentration of fluid. The higher the concentration the thinner the double layer and consequently the smaller the relaxation and EDL overlap effect. The other contributor electrostatic repulsion is basically columbic force in not directly related to concentration of fluid. But when EDL is formed around a charged body it practically muffles the field created by the charge. Outside the double the columbic force becomes very weak and less important. So concentration of electrolyte plays a vital role in determining the electrical drag force acting on a submerged charged particle. It must be noted that in these models the channel radius (b) is considered as the length scale and the inverse Debye length is also scaled using channel radius for all simulations. The channel radius is considered to be constant and the value of κb is changed to change solution concentration.

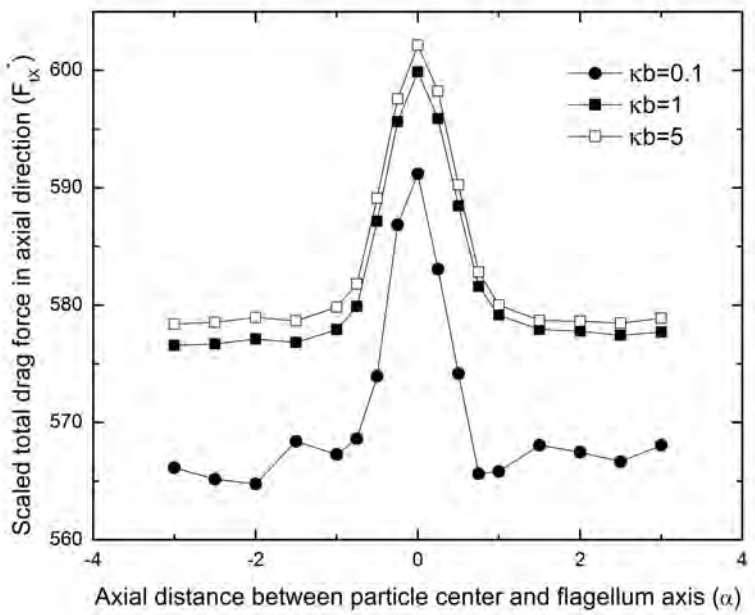

Figure 4.23: Variation of scaled total axial drag force for different solution concentration, κb=0.1,1,5. Potential on particle and flagellum ψ^*= -1, u^*=0.45

4.3.1 Variation of drag force

Variation to axial drag force on particle with concentration is depicted in Fig 4.23. All the three plots in this figure are similar in nature suggesting that, variation in concentration just affect the value of drag force not in their behavior. With the increase of concentration the drag force increases. This could be little confusing since, with the increase of concentration there are more ions in the solution and they quickly surround the charged particle and flagellum and produce thinner double layer. The relaxation effect becomes less prominent and the electrical drag force should decrease. However with the increase of concentration the surface charge density of the particle and flagellum both increase. It needs to be mentioned that surface charge density of the particle is calculated from another model considering a spherical particle of surface potential -1 in an infinite solution of similar concentration. Coupled Poisson, Nernst-Planck equation is solved to evaluate the surface charge density on the particle. As the surface charge density increases with concentration though local electric field decreases the total axial drag increases with concentration of solution.

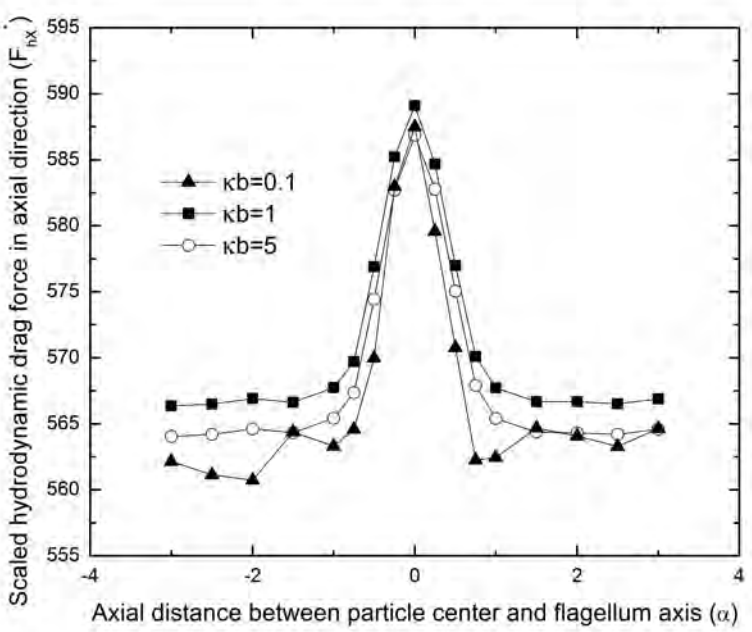

Figure 4.24: Variation of scaled hydrodynamic drag force in axial direction for different solution concentration, κb=0.1,1,5 in axial direction. Potential on particle and flagellum ψ^*= -1, u^*=0.45

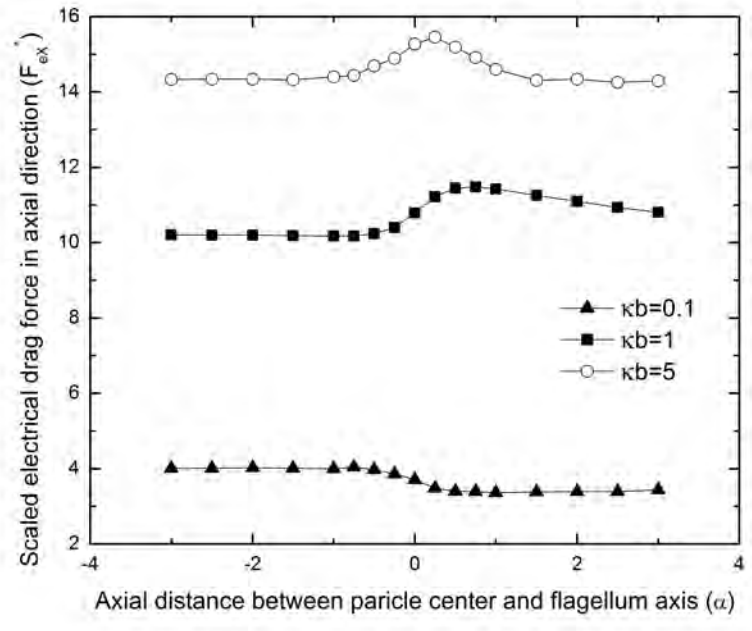

Figure 4.25: Variation of scaled electrical drag force for different solution concentration, κb=0.1,1,5 in axial direction. Potential on particle and flagellum ψ^*= -1, u^*=0.45

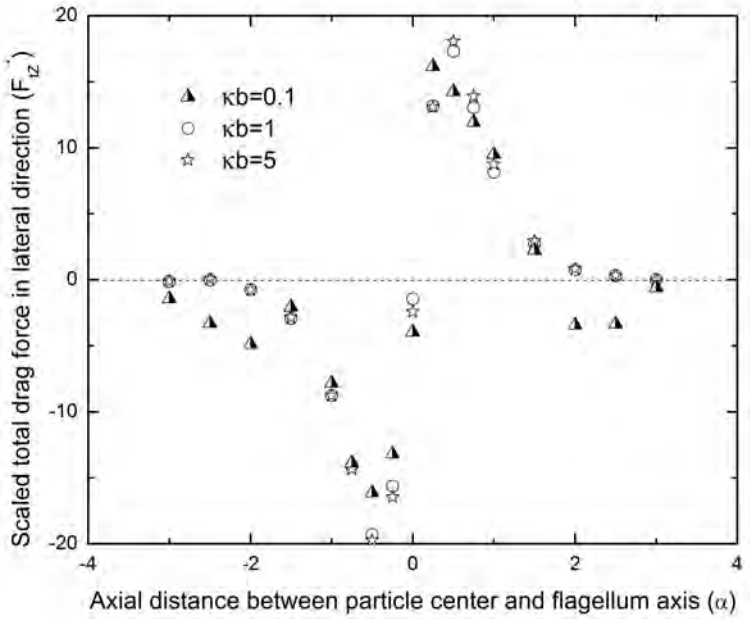

Figure 4.26: Variation of scaled total lateral drag force for different solution concentration, κb=0.1,1,5. Potential on particle and flagellum ψ^*= -1, u^*=0.45

To understand how much increase occurs in electrical drag with the increase of concentration, hydrodynamic and electrical drag forces for varying concentration is illustrated in Fig 4.24 and Fig 4.25. It clearly shows that with the increase of concentration electrical drag force increases from around 3 to 15. It also suggests that the electrical drag force is slightly different at flagellum upstream and downstream at lower concentration (κb=0.1,1). Relaxation and EDL overlap could be the reason behind it which will be discussed on later section. Moreover there is a small variation in hydrodynamic drag force. This is caused by the electrical body force acting on the fluid.

The variation of lateral drag force for varying concentration is plotted in Fig 4.26. Here variation in concentration is not that much prominent in z direction. Although concentration does not vary the hydrodynamic drag force in lateral direction (z direction) but it affects the electrical drag force in lateral direction. Fig 4.27 shows the variation of electrical drag force in lateral direction for varying concentration. It clearly shows that, with the increase of concentration electrical drag increase first and then at high concentration (κb=5) falls even it becomes positive that is, it push the particle upward against the repulsion force. So at lower concentration electrostatic repulsion is dominant and the drag force is push the particle away form

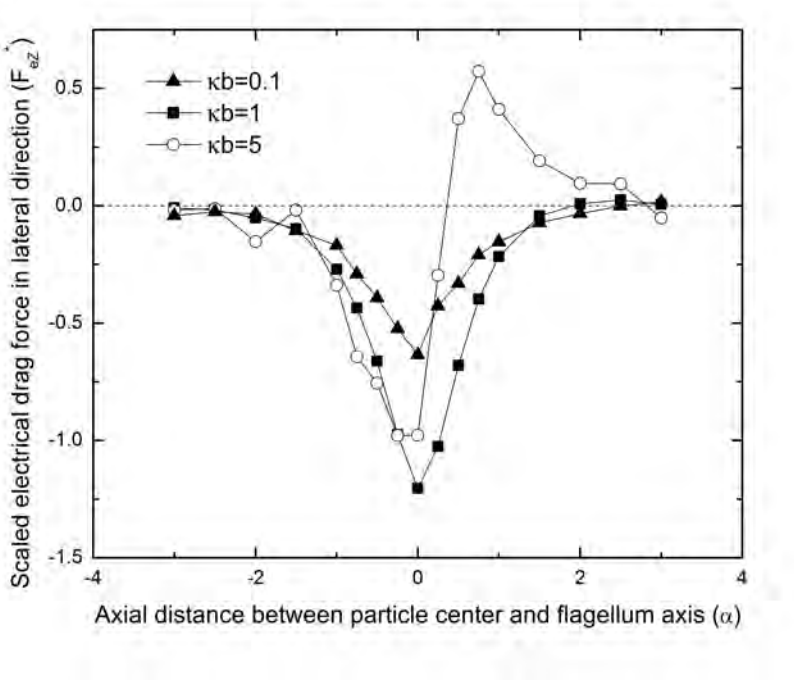

Figure 4.27: Variation of scaled electrical drag force in lateral direction for different solution concentration, κb=0.1,1,5. Potential on particle and flagellum ψ^*= -1, u^*=0.45

the flagellum. With the increase of concentration electrostatic repulsion becomes stronger due to increased surface charge density on both the particle and flagellum. But when concentration increases more repulsive force loose its dominance and relaxation and EDL overlap start to become prominent. Both of them gather more positive ion above the particle and local electric field produces a positive electrical drag. Another thing that affect electric repulsion is thinner electric double layer at higher concentration. With the increase of concentration the electric double layer becomes thinner the potential on flagellum and particle are muffled by the surrounding ions and they can hardly feel the presence of other. A graphical comparison of the EDL thickness is presented in Fig 4.28 for better understanding. Another figure, Fig: **??** shows the velocity distribution inside the channel for different concentration for a good insight of velocity distribution.

4.3.2 Effect of relaxation

Relaxation shows strong dependency on concentration. It is already discussed that, with the increase of concentration the EDL becomes thinner and the ions are more tightly bonded inside the EDL. Consequently the deformation of EDL

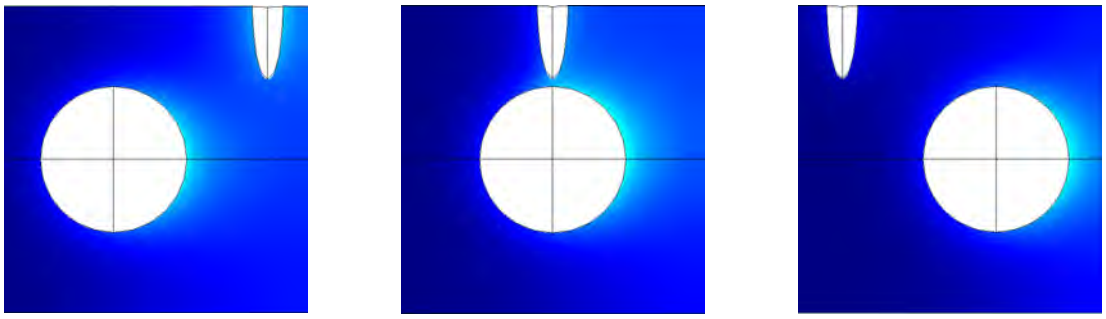

(a) κb=0.1, α=-1, ψ^*=-1 (b) κb=0.1, α=0, ψ^*=-1 (c) κb=0.1, α=1, ψ^*=-1

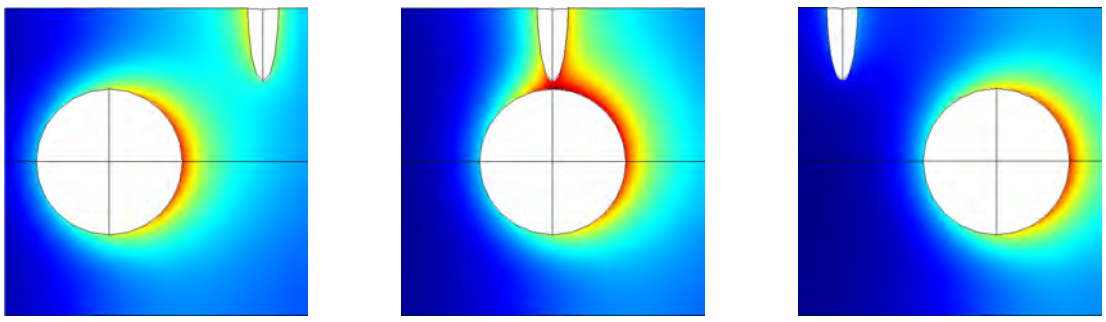

(d) κb=1, α=-1, ψ^*=-1 (e) κb=1, α=0, ψ^*=-1 (f) κb=1, α=1, ψ^*=-1

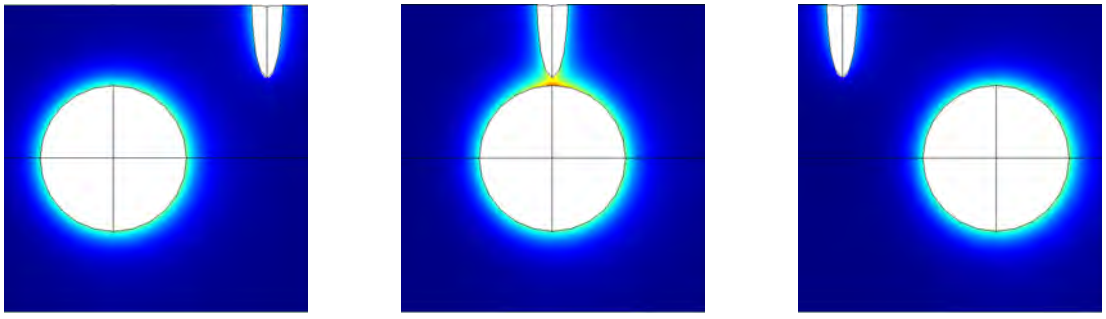

(g) κb=5, α=-1, ψ^*=-1 (h) κb=5, α=0, ψ^*=-1 (i) κb=5, α=1, ψ^*=-1

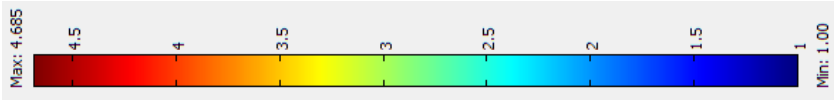

(j) Scale for color plot of scaled positive ion concentration around the particle

Figure 4.28: Variation of scaled positive ion concentration for different solution concentration, at different axial distance between particle center and flagellum axis

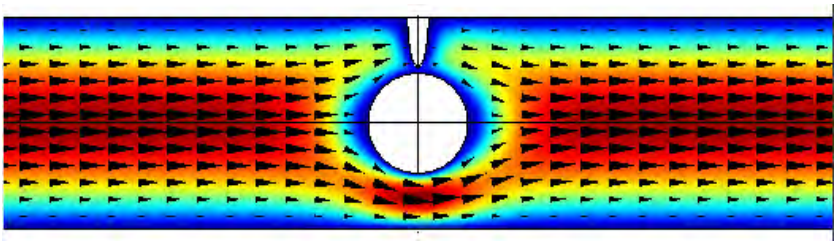

(a) Separation distance β=0.5, Axial distance α=0,κb=0.1, U=0.45

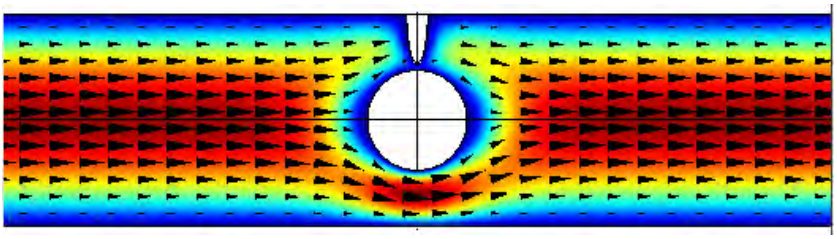

(b) Separation distance β=0.5, Axial distance α=0,κb=1, U=0.45

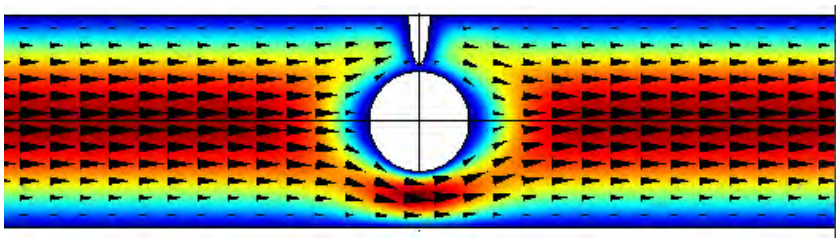

(c) Separation distance β=0.5, Axial distance α=0,κb=5, U=0.45

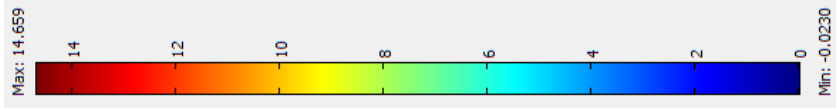

(d) Scale for color plot

Figure 4.29: Scaled velocity distribution throughout the channel for different solution concentration. (Arrow plot is showing the radial velocity distribution)

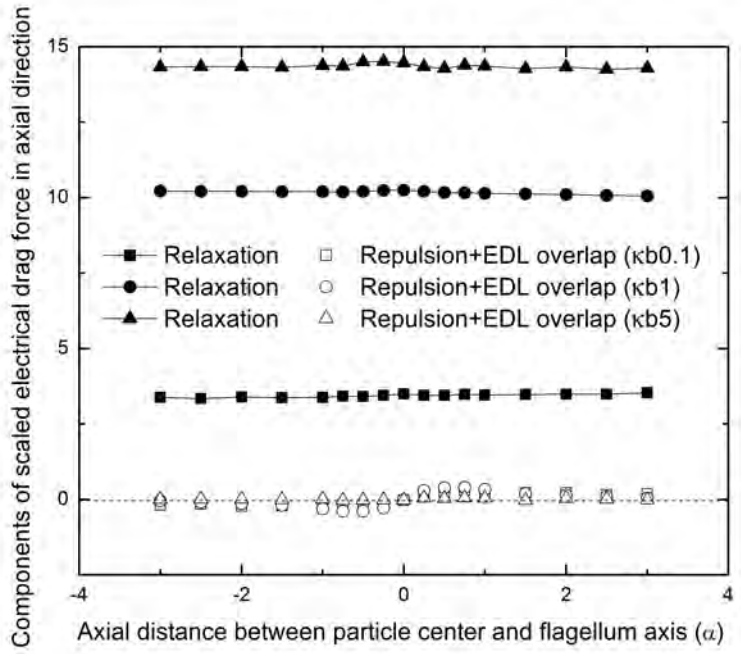

Figure 4.30: Contribution of different electrokinetic phenomena on scaled total electrical drag force in axial direction for varying solution concentration, κb=0.1,1,5 ψ^*=-1

becomes less possible and local electric field around the particle decreases. But at the same time surface charge density increases that increase the electrical drag force. To understand the relaxation effect, relaxation of a charged particle confined in an uncharged cylindrical channel having uncharged flagellum for different concentration is modeled. Since the only charged object is the particle so there will no other electrical effect except relaxation. Another model has been solved with charged particle and flagellum with no induced flow. In absence of flow there will be no distortion of EDL caused by electric field (some distortion will take place due to the presence of flagellum)and only the effect of electrostatic repulsion and undisturbed EDL overlap will be obtained.

Fig 4.30 shows the variation of electrical drag force caused by charge relaxation and combined effect of electrostatic repulsion and undisturbed EDL overlap with concentration. It shows that, with the increase of κb i.e concentration the relaxation drag increases. The drag force caused by the combined effect of electrostatic repulsion and undisturbed EDL overlap increases first with the increase of concentration and decreases again at higher concentration.

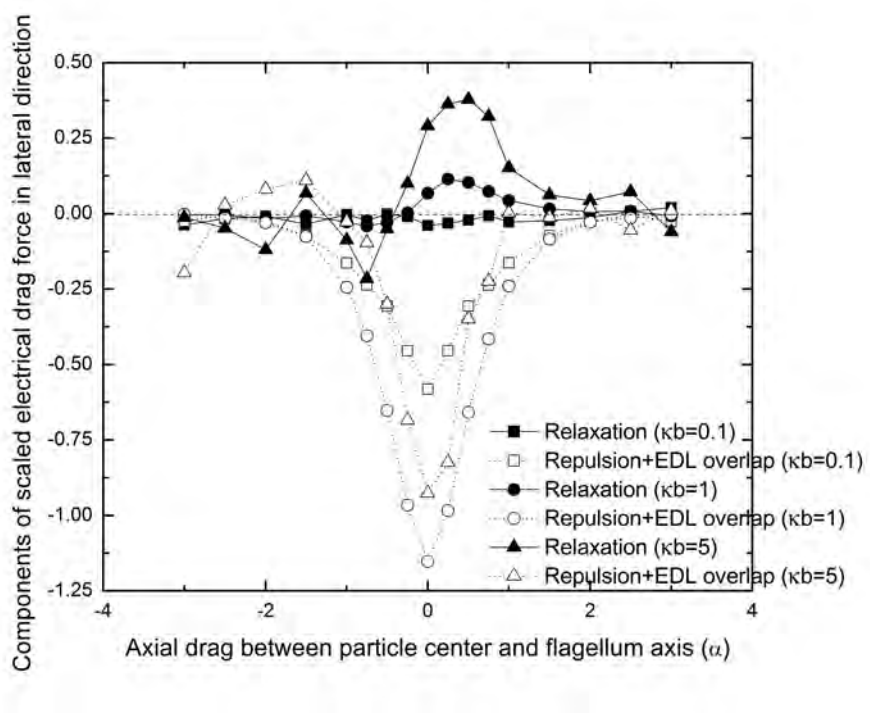

Figure 4.31: Contribution of different electrokinetic phenomena on scaled total electrical drag force in lateral direction for varying solution concentration, κb=0.1,1,5, ψ^*=-1

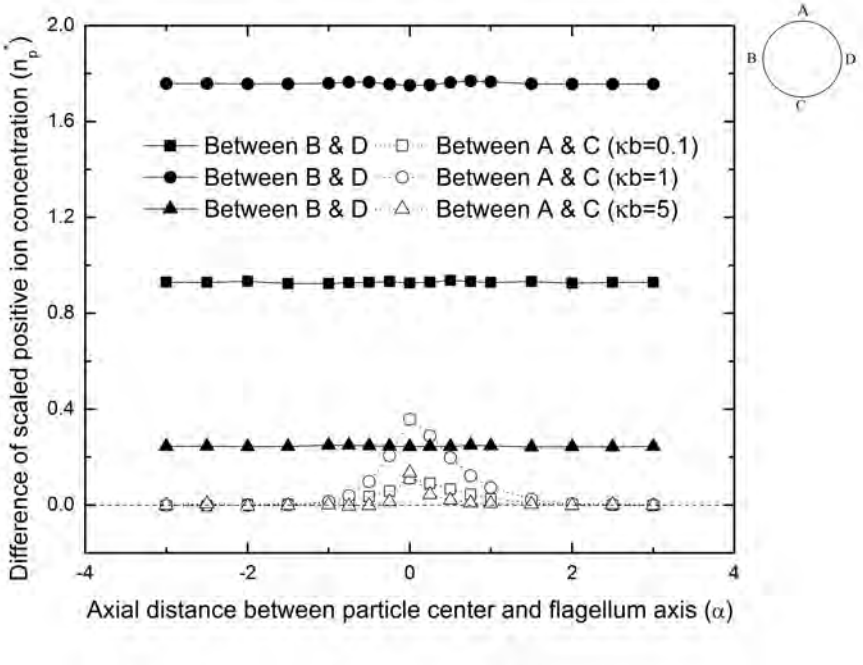

Figure 4.32: Difference of scaled positive ion concentration at different points on the charged particle while flagellum is considered uncharged, ψ^*=-1

Fig 4.31 shows the variation of electrical drag force in lateral direction caused by relaxation and combined effect of electrostatic repulsion and undisturbed EDL overlap with concentration. In lateral direction relaxation has very low effect and it basically oppose the electrostatic repulsion which is prominent in lateral direction. This thing continues with the increase of concentration. At higher concentration relaxation drag force increases significantly. Relaxation drag force is positive and mostly created in the vicinity of flagellum downstream. Far from the flagellum relaxation drag force becomes near zero for all solute concentration. The presence of flagellum even when uncharged distort the EDL produced around the particle and accumulate more positive charge at the flagellum side. With the increase of concentration the negative drag produced by the combined effect of repulsion and undisturbed EDL overlap increases. The reason is the increased surface charge density at higher concentration. Though EDL overlap decreases with the increase of concentration but the increase in surface charge density seems to be more prominent to increase the repulsion.

Concentration difference of positive ion between four different points A and C, B and D for different concentration is illustrated in Fig 4.32. How the relaxation effect diminishes with the increases of concentration can be easily explained from here. It is clear that while keeping all the other parameters constant, with the increase of concentration the difference of ions around the particle reduces rapidly. This difference establishes a local electric field which in terns produce electrical drag force. Things stated above holds good for κb= 1 and 5. But at very low concentration (κb=0.1) things are different. It was expected, for κb=0.1 the difference of positive ion concentration will be highest. But surprisingly it is lower than that for κb=1. Very low concentration and surface charge is the reason behind this phenomena. Both of these causes the EDL to disperse through out the whole channel. This makes the concentration nearly uniform around the particle. Another interesting fact is the concentration difference between A and C. The presence of uncharged flagellum accumulates positive ion around it an produce positive drag that oppose both the hydrodynamic drag and repulsive force in case of charged flagellum.
Fig: **??** shows the concentration distribution along the channel at different concentration. At lower concentration there are variation of concentration throughout the channel while at higher concentration, ion distribution throughout the channel is nearly uniform except at the vicinity of particle and flagellum. This causes the relaxation and EDL overlap to become less significant with the increase of concentration. Fig: **??** shows the potential field inside the channel. It shows with the

increase of concentration potential across the particle varies significantly resulting higher electric field. This electric field results in higher electrical drag force at higher concentration.

4.3.3 Effect of EDL overlap

At higher concentration the effect of EDL overlap is very low as there is not much thick EDL is available. Fig 4.35 shows the contribution of three different electrokinetic phenomena on axial electrical drag force at different concentration (κb=0.1,1,5). One of them is relaxation drag force which is discussed in previous subsection. The other two results are the total electrical drag force in axial direction and the drag force produced by the combination of electrostatic repulsion and undisturbed EDL overlap. The contribution of the last one is near zero at every concentration. The difference between relaxation drag force and total drag force gives the effect of distorted EDL overlap caused by the flow. Even the presence of uncharged flagellum distort the double layer. The total drag force is basically comprises of relaxation drag force, repulsion drag force and the force produced by distorted (caused by both flow and charged flagellum) EDL overlap. It clearly shows, that at higher concentration the difference between relaxation drag force and total drag force decreases. At higher concentration the overlap effect is visible only at the vicinity of the flagellum but at lower concentration it has good affect even away form the flagellum too. Thinner EDL at higher concentration is the reason behind it. At κb=0.1 the EDL overlap is more prominent at flagellum upstream and at κb=1 it is prominent at flagellum down stream. Similar phenomena occurs in lateral direction too. Fig 4.36 shows the concentration gradient of positive ion between B and D point i.e in axial direction for two different models. One gives the relaxation effect (model with charged particle and uncharged flagellum) and the other one is model for present problem. At lower concentration κb= 0.1,1 there is a certain difference between these two curves showing the EDL overlap effect. But at higher concentration curves for both the models overlap indicating with the increase of concentration EDL overlap also becomes negligible like relaxation. Interestingly the difference of ion concentration is less for κb=0.1 than for κb=1. Very dilute solution creates a large EDL and the concentration distribution becomes more or less uniform inside it. This is the reason behind this behavior.

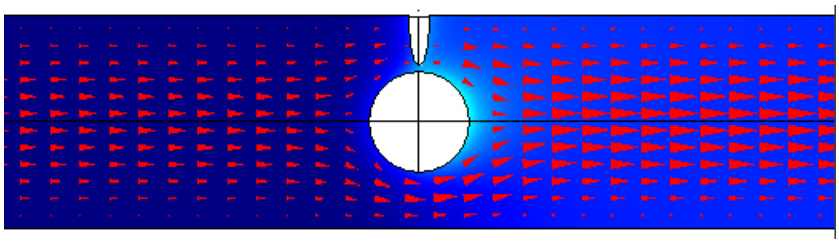

(a) Separation distance β=0.5, Axial distance α=0,κb=0.1, U=0.45

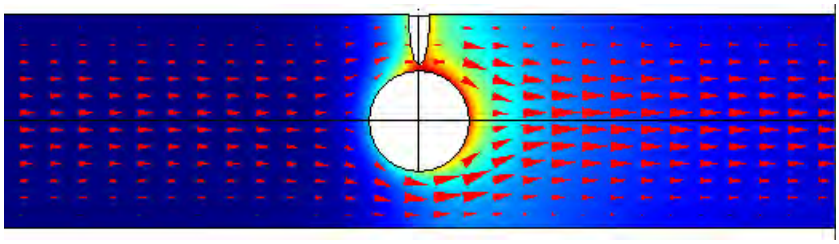

(b) Separation distance β=0.5, Axial distance α=0,κb=1, U=0.45

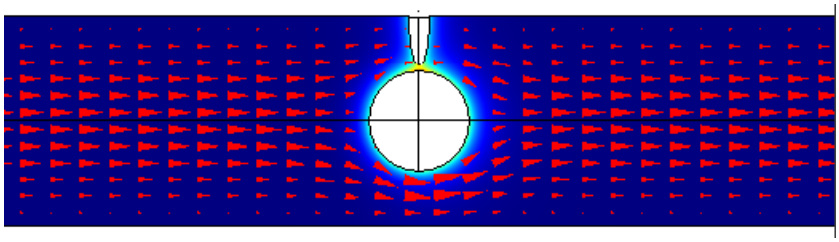

(c) Separation distance β=0.5, Axial distance α=0,κb=5, U=0.45

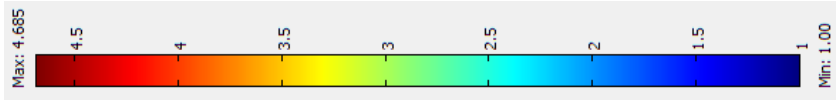

(d) Scale for concentration distribution color plot

Figure 4.33: Scaled positive ion concentration distribution throughout the channel for different solution concentration (Arrow plot is showing the convective flux of positive ion)

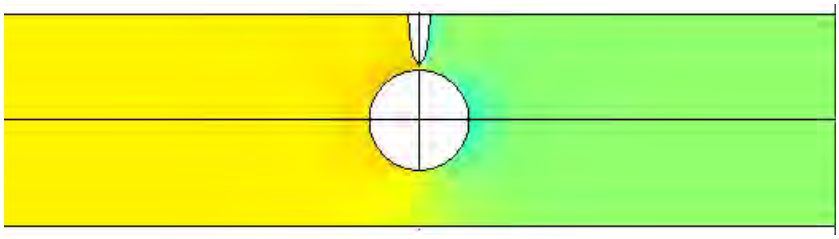

(a) Separation distance β=0.5, Axial distance α=0,κb=0.1, U=0.45

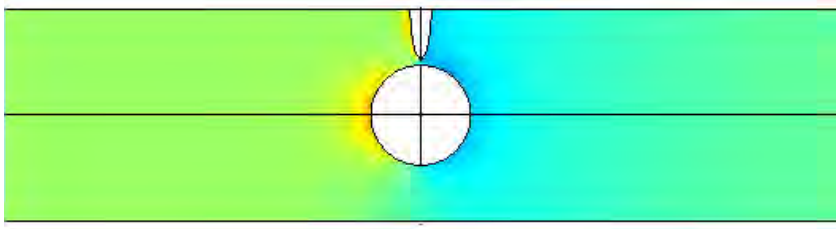

(b) Separation distance β=0.5, Axial distance α=0,κb=1, U=0.45

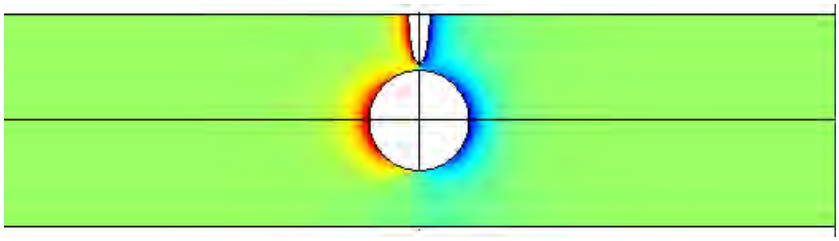

(c) Separation distance β=0.5, Axial distance α=0,κb=5, U=0.45

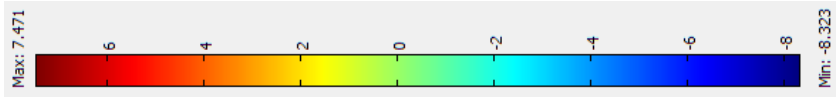

(d) Scale for color plot of electric field distribution

Figure 4.34: Electric field distribution for different solution concentration

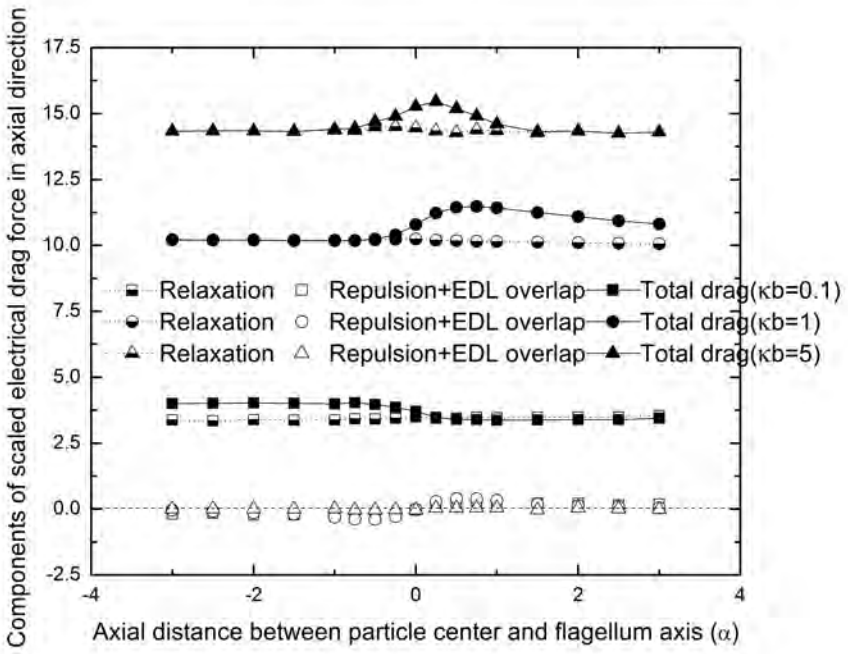

Figure 4.35: Scaled axial electrical drag produced by different electrokinetic phenomena at different concentration, κb=0.1,1,5. ψ^*=-1, u^*=0.45

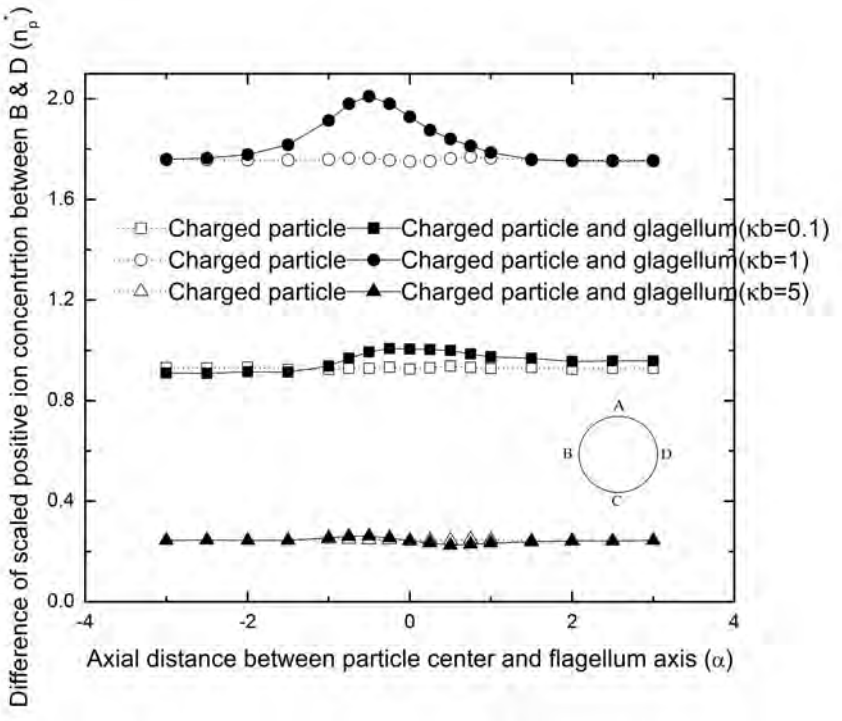

Figure 4.36: Difference of scaled positive ion concentration between point B and D over the charged particle at varying concentration, κa=1,5,10, ψ=-1, u^*=0.45

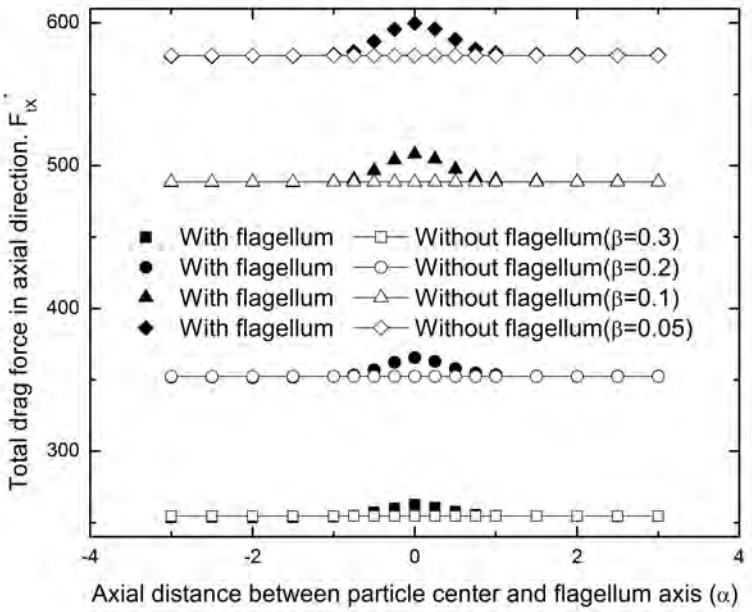

Figure 4.37: Scaled drag force in axial direction on a charged particle (ψ^*=-1) confined in a channel having similarly charged flagellum and no flagellum, u^*=0.45

4.4 Effect of charged flagellum

Presence of charged flagellum might be the most influential event in the present problem. If the flagellum was not present any disturbance in the lateral direction would be absent. Drag force in axial direction is expected to be uniform throughout the channel length. Since there would be no charged object rather than the particle only, there will be no EDL overlap or electrostatic repulsion.

4.4.1 Drag forces

The variation of axial drag in presence and absence of charged flagellum for different size ratio is illustrated in Fig 4.37. It shows that presence of flagellum increase the drag on the particle at the vicinity of the flagellum. So the particle will feel more drag and more force will be required to keep the particle stationary near the flagellum. If there was no flagellum the drag is more or less constant through out the channel. It is quite understandable as the presence of flagellum disturbs the flow pattern and reduce the cross sectional area. As a result the local fluid velocity near the flagellum increases and consequently increases the drag. It is also evident from the figure that The greater the flagellum length the higher the increase of drag. The

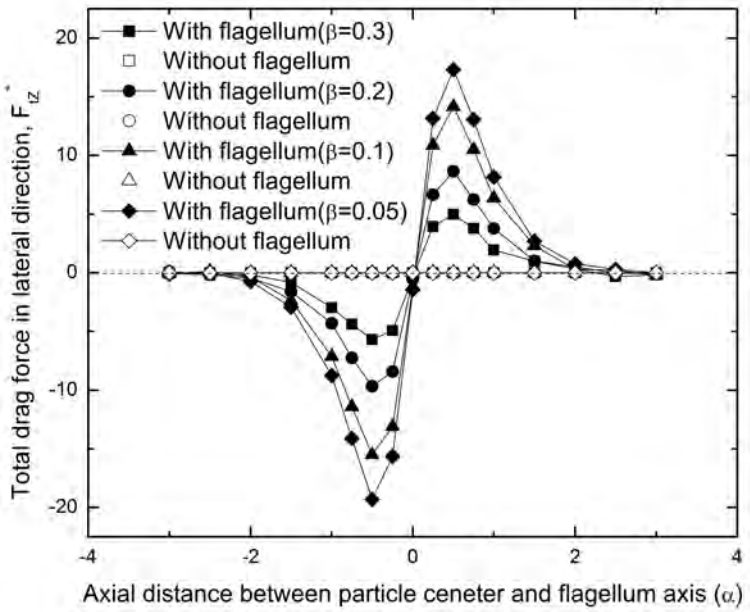

Figure 4.38: Scaled drag force in lateral direction on a charged particle (ψ^*=-1) confined in a channel having similarly charged flagellum and no flagellum, u^*=0.45

variation of lateral drag is illustrated in Fig 4.38. It clearly shows that in absence of flagellum there is almost no drag force in lateral direction. So it is clear that drag force in lateral direction is solely created by the presence of flagellum. So the presence of flagellum will cause a particle to move away from the centerline.

4.4.2 Drag factor

Presence of flagellum whether charged of uncharged drastically affect the drag factor (K_2). The variation of drag factor at varying axial distance between particle and flagellum for uncharged particle and uncharged flagellum, charged particle and uncharged flagellum , charged particle and flagellum is shown in Fig 4.39 The size ration is considered to be λ=0.475, and for charged cases the concentration is assumed to be κb=1. These two parameters are so chosen since for them we get the maximum effect. It is clear form the figure presence of uncharged flagellum in a channel carrying an uncharged particle, only increases the drag in the vicinity of the flagellum. away from the flagellum the drag factor is more or less equal to the drag factor for an uncharged spherical particle inside a channel. But if the particle is charge there is upshift of drag factor throughout the whole channel. This excess drag is caused by the relaxation effect which is already discussed in literature. The

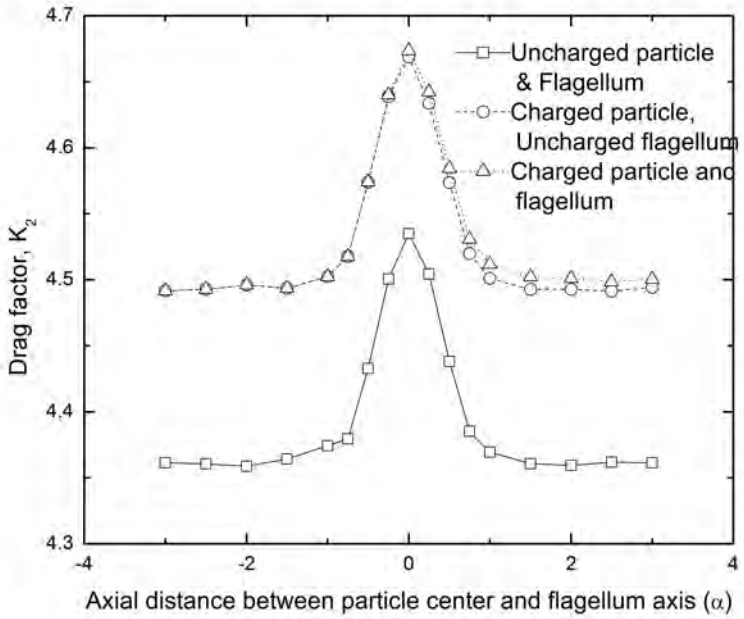

Figure 4.39: Drag factor at various axial distance between particle and flagellum for a)uncharged particle and flagellum, b)charged particle, uncharged flagellum and c)charged particle and flagellum, ψ^*=-1, κb=1, λ=0.475, u^*=0.45

increase in drag force caused by relaxation is also discussed in previous sections. For charged particle and flagellum the drag force increases a little more. But this increasing happens at the flagellum downstream. Distorted EDL overlap at flagellum downstream is the reason behind this. Fluid flow causes the EDL to distort and more ions accumulate at flagellum downstream. They increase the drag and eventually drag factor.

Drag factor at different solution concentration is plotted in Fig 4.40 Here also the size ration is assumed to be 0.475 to achieve the maximum effect. The graph is plotted for three different cases. Uncharged particle and flagellum, charged particle and uncharged flagellum, charged particle and flagellum. Solution concentration has no effect in the case of uncharged particle and flagellum and hence is constant. But for other two cases with the increase of concentration drag factor increases. It is already known that with the increase of concentration electrical drag on the particle increases, which increases the total drag on the particle. As a result the drag factor increases. Drag factor for charged flagellum is visibly higher than that for uncharged flagellum. Overlapping of EDL causes this extra drag force. It should be mentioned that, in this figure all the drag force is calculate while the particle center is situated

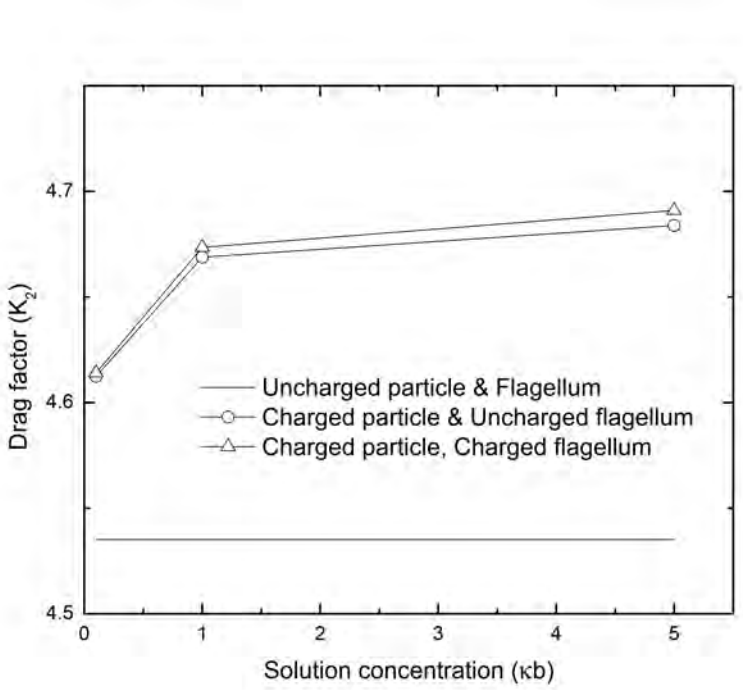

Figure 4.40: Drag factor as a function of solution concentration (κb) for a)uncharged particle and flagellum, b)charged particle, uncharged flagellum and c)charged particle and flagellum, ψ^*=-1,λ=0.475, u^*=0.45

on the flagellum axis. So it is expected that at flagellum downstream the difference between the drag factors could be higher.

Drag factor for different size ratio at different solution concentration (κb) is plotted in Fig 4.41 The bar chart clearly shows that with the increase of λ drag factor increases for every κb. This means the higher the particle size the higher will be the drag factor. Another thing is that for the same size ratio with the increase of κb drag factor increases. But the increment is visible at higher size ratio (λ). At higher λ the separation gap between the particle and flagellum decreases which facilitates more EDL overlap. This seems to be the reason behind it. The excess drag caused by the presence of charged flagellum at different κb is plotted in Fig 4.42 Excess drag is calculate by subtracting the drag factor for and uncharged particle in an uncharged cylindrical channel form the drag produced on a charged particle confined in a cylindrical channel containing charged flagellum. Here excess drag produced increases with the increase of both size ration and concentration

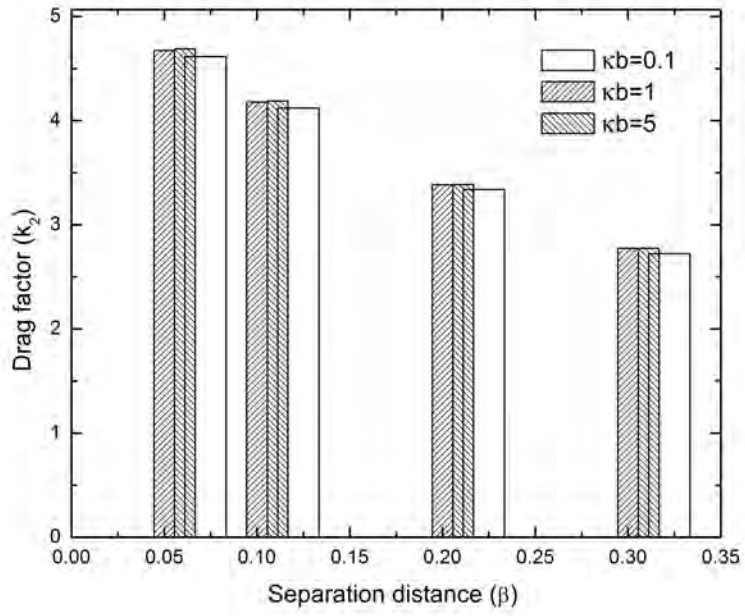

Figure 4.41: Drag factor as a function of separation distance (β)for different concentration κb=0.1,1,5. Particle and flagellum surface potential, ψ^*=-1. u^*=0.45

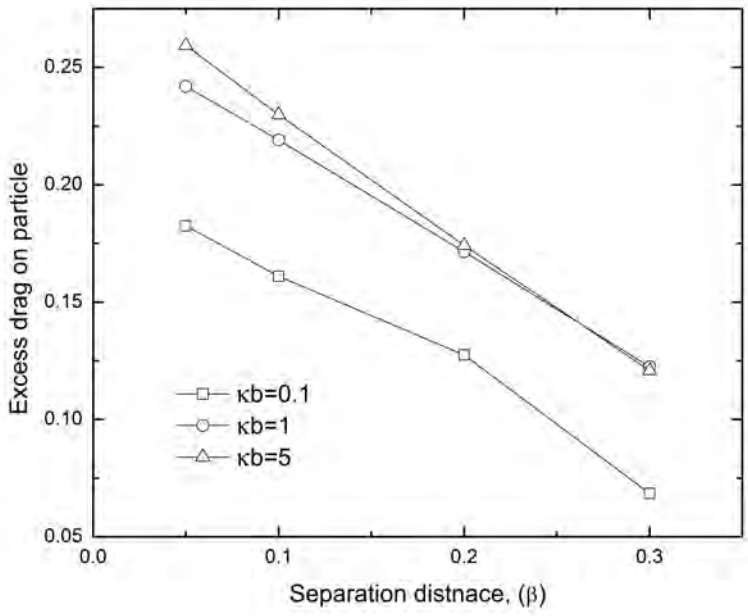

Figure 4.42: Excess drag for relaxation and EDL overlap as function of separation distance, β at different κb. ψ^*=-1, u^*=0.45

Chapter 5

CONCLUSION AND RECOMMENDATIONS

5.1 Concluding remarks

Hindered motion of charged spherical particle through a pressure driven flow inside micropore having charged or uncharged surface is a continually developing and enriching field. Numerous authors are devoting themselves in explaining various electrokinetic and hydrodynamic behavior of such systems due to its strong resemblance in various biological and chemical phenomena. Various channel wall geometry and particle-wall surface charge configuration is yet to be explored. All the studies available considered centerline approximation as well as straight cylindrical channel. Complex 3D nature and robustness of coupled solution make these problems little intimidating.

The hindered motion of a charged spherical particle inside a cylindrical channel having flagellum like charged surface irregularity is studied here. For simplicity the length of the flagellum is considered to be equal to the radius of the particle and they are assumed to be similarly charged. Firstly the electrokinetic and hydrodynamic interactions between charged particle and flagellum is studied for different size ratio (λ) keeping the solution concentration constant (κb=1). Later the effect of concentration is analyzed. Lastly the effect of presence of flagellum (charged and uncharged) is analyzed. From the study the following concluding remarks could be inferred:

- Total axial and lateral drag on the particle increases with the increase of size ratio (λ) or the decrease of separation gap between particle and flagellum. For

any λ the total axial drag force is uniform along the whole channel except at the vicinity of the flagellum where the drag force increases, reaches at a maximum value and then decreases again to the average value at flagellum downstream. The % increment in drag factor from the average value increases with the increase of λ.

- Electrical drag on the particle in axial direction is caused by the combination of electrostatic repulsion between the particle and flagellum, relaxation and double layer overlap. Among these three, relaxation and EDL overlap always increase electrical drag in axial direction and electrostatic repulsion, at flagellum upstream decrease and at downstream increase the drag. For this reason axial electrical drag is higher at flagellum downstream than upstream. Electrical drag in lateral direction is symmetric in nature and maximum when the particle is just below the flagellum. Electrical drag in both directions increase with the increase of λ

- Presence of charge on both particle and flagellum increase the drag force on the particle. But the % increase in lateral drag is higher than that of axial drag. If the particle and flagellum are oppositely charged axial drag force is less at flagellum downstream than the drag force for likely charged particle and flagellum or charged particle, uncharged flagellum. For oppositely charged particle and flagellum lateral drag is also reduced.

- Drag force caused by the relaxation of EDL is always the total drag in flow direction. Relaxation drag is the most prominent contributor in electrical drag in axial direction. It's contribution is so high that it basically determines the direction and value of axial electrical drag. But in lateral direction relaxation is dominated by repulsion effect.

- With the increase of concentration both the axial and lateral drag force increase. Though at higher concentration EDL becomes thinner and relaxation becomes less prominent, increased surface charged density for constant surface potential is the reason behind it. With the increase of concentration ions become more tightly bonded to the particle and concentration difference across the particle decreases. This reduces relaxation and EDL overlap. Even at higher concentration repulsion force also decreases.

- Presence of flagellum increases the drag factor at the vicinity of the flagellum. Drag factor is also affected by the concentration. For any λ drag increase with the increase of concentration. But this is hard to observe at lower λ

5.2 Future work

Couple solution of governing equations and 3D nature of the developed model enable it to deal with various channel geometry and particle position for a wide range of Debye length and surface charge condition. Using this model findings could be extended in the following directions.

- A single particle and flagellum system is considered here for simplicity. But a multiparticle, multiflagellum geometry could be developed to study the hydrodynamic and electrokinetic interaction among then which is closer to real case.

- The particle could be place at eccentric position to find the excess drag factor due to eccentricity which is yet to be clearly understood. Sure uneven velocity profile at eccentric position will relax the EDL in different way and drag factor will be affected by that.

- The base radius of the flagellum is assumed to be constant in this problem. But surely the flagellum base influence the drag on the particle both hydrodynamically and electrokinetically. So effect for various flagellum length to flagellum base radius ratio could be studied.

- Various shaped (dumbbell, cylindrical, circular disk, cubes, parallelepipeds, needles and thin plates) object can be used instead of spherical particle to study their behavior.

- Different shaped flagellum (tilted, serpentine) could be studied.

- All the capillaries in living bodies are actually curved and elastic in nature. To accommodate this curved channel with elastic properties could be studied.

- Soft particle along with particle rotation dew to eccentricity and tangential flow could be introduced.

Bibliography

[1] Anderson, J. L., and Quinn, J. A. Restricted transport in small pores: a model for steric exclusion and hindered particle motion. *Biophysical Journal 14*, 2 (1974), 130–150.

[2] Bean, C. P. The physics of porous membranes–neutral pores. *Membranes 1* (1972), 1.

[3] Bear, J., and Bachmat, Y. *Introduction to modeling of transport phenomena in porous media*, vol. 4. Springer, 1990.

[4] Ben Richou, A., Ambari, A., and Naciri, J. Correction factor of the stokes force undergone by a sphere in the axis of a cylinder in uniform and poiseuille flows. *The European Physical Journal Applied Physics 24*, 02 (2003), 153–165.

[5] Bhalla, G., and Deen, W. Effects of charge on osmotic reflection coefficients of macromolecules in fibrous membranes. *Biophysical journal 97*, 6 (2009), 1595–1605.

[6] Bhalla, G., and Deen, W. Effects of charge on osmotic reflection coefficients of macromolecules in porous membranes. *Journal of colloid and interface science 333*, 1 (2009), 363–372.

[7] Bowen, W. R., and Sharif, A. O. Transport through microfiltration membranesparticle hydrodynamics and flux reduction. *Journal of colloid and interface science 168*, 2 (1994), 414–421.

[8] Bowen, W. R., and Sharif, A. O. The hydrodynamic and electrostatic interactions on the approach and entry of a charged spherical particle to a charged cylindrical pore in a charged planar surface with implications for membrane separation processes. *Proceedings of the Royal Society of London. Series A: Mathematical, Physical and Engineering Sciences 452*, 1952 (1996), 2121–2140.

[9] Bungay, P. M., and Brenner, H. The motion of a closely-fitting sphere in a fluid-filled tube. *International Journal of Multiphase Flow 1*, 1 (1973), 25–56.

[10] Burns, D. B., and Zydney, A. L. Contributions to electrostatic interactions on protein transport in membrane systems. *AIChE journal 47*, 5 (2001), 1101–1114.

[11] Chellam, S., and Wiesner, M. R. Particle transport in clean membrane filters in laminar flow. *Environmental science & technology 26*, 8 (1992), 1611–1621.

[12] Chun, M.-S., and Phillips, R. J. Electrostatic partitioning in slit pores by gibbs ensemble monte carlo simulation. *AIChE journal 43*, 5 (1997), 1194–1203.

[13] Dechadilok, P., and Deen, W. Hindrance factors for diffusion and convection in pores. *Industrial & engineering chemistry research 45*, 21 (2006), 6953–6959.

[14] Dechadilok, P., and Deen, W. Electrostatic and electrokinetic effects on hindered convection in pores. *Journal of colloid and interface science 338*, 1 (2009), 135–144.

[15] Dechadilok, P., and Deen, W. Electrostatic and electrokinetic effects on hindered diffusion in pores. *Journal of Membrane Science 336*, 1 (2009), 7–16.

[16] Deen, W. Hindered transport of large molecules in liquid-filled pores. *AIChE Journal 33*, 9 (1987), 1409–1425.

[17] Deen, W., et al. What determines glomerular capillary permeability? *Journal of Clinical Investigation 114*, 10 (2004), 1412–1414.

[18] Eggleton, C. D., and Popel, A. S. Large deformation of red blood cell ghosts in a simple shear flow. *Physics of Fluids (1994-present) 10*, 8 (1998), 1834–1845.

[19] Ennis, J., and Anderson, J. Boundary effects on electrophoretic motion of spherical particles for thick double layers and low zeta potential. *Journal of colloid and interface science 185*, 2 (1997), 497–514.

[20] Ennis, J., Zhang, H., Stevens, G., Perera, J., Scales, P., and Carnie, S. Mobility of protein through a porous membrane. *Journal of membrane science 119*, 1 (1996), 47–58.

[21] Ferry, J. D. Statistical evaluation of sieve constants in ultrafiltration. *The Journal of general physiology 20*, 1 (1936), 95–104.

[22] Haberman, W. L., and Sayre, R. M. Motion of rigid and fluid spheres in stationary and moving liquids inside cylindrical tubes. Tech. rep., DTIC Document, 1958.

[23] Happel, J., and Brenner, H. *Low Reynolds number hydrodynamics: with special applications to particulate media*, vol. 1. Springer, 1983.

[24] Haraldsson, B., Nyström, J., and Deen, W. Properties of the glomerular barrier and mechanisms of proteinuria. *Physiological reviews 88*, 2 (2008), 451–487.

[25] Higdon, J., and Muldowney, G. Resistance functions for spherical particles, droplets and bubbles in cylindrical tubes. *Journal of Fluid Mechanics 298* (1995), 193–210.

[26] Hsu, J.-P., and Liu, B.-T. Electrical interaction energy between two charged entities in an electrolyte solution. *Journal of colloid and interface science 217*, 2 (1999), 219–236.

[27] Johnson, E. M., Berk, D. A., Jain, R. K., and Deen, W. Diffusion and partitioning of proteins in charged agarose gels. *Biophysical journal 68*, 4 (1995), 1561.

[28] Keh, H., and Anderson, J. Boundary effects on electrophoretic motion of colloidal spheres. *Journal of Fluid Mechanics 153* (1985), 417–439.

[29] Kundu, P., and Cohen, I. *Fluid Mechanics. 2004*. Elsevier Academic Press, 2008.

[30] Liu, Y., and Liu, W. K. Rheology of red blood cell aggregation by computer simulation. *Journal of Computational Physics 220*, 1 (2006), 139–154.

[31] Masliyah, J. H., and Bhattacharjee, S. *Electrokinetic and colloid transport phenomena*. John Wiley & Sons, 2006.

[32] Minerick, A. R., Zhou, R., Takhistov, P., and Chang, H.-C. Manipulation and characterization of red blood cells with alternating current fields in microdevices. *Electrophoresis 24*, 21 (2003), 3703–3717.

[33] Mitchell, B. D., and Deen, W. Theoretical effects of macromolecule concentration and charge on membrane rejection coefficients. *Journal of membrane science 19*, 1 (1984), 75–100.

[34] Mitragotri, S. Modeling skin permeability to hydrophilic and hydrophobic solutes based on four permeation pathways. *Journal of Controlled Release 86*, 1 (2003), 69–92.

[35] Nakao, S., Osada, H., Kurata, H., Tsuru, T., and Kimura, S. Separation of proteins by charged ultrafiltration membranes. *Desalination 70*, 1 (1988), 191–205.

[36] Odde, D. Diffusion inside microtubules. *European biophysics journal 27*, 5 (1998), 514–520.

[37] Pappenheimer, J., Renkin, E., and Borrero, L. Filtration, diffusion and molecular sieving through peripheral capillary membranes, 1951.

[38] Pozrikidis, C. Numerical simulation of the flow-induced deformation of red blood cells. *Annals of Biomedical Engineering 31*, 10 (2003), 1194–1205.

[39] Pujar, N. S., and Zydney, A. L. Electrostatic effects on protein partitioning in size-exclusion chromatography and membrane ultrafiltration. *Journal of Chromatography A 796*, 2 (1998), 229–238.

[40] Quddus, N., Moussa, W., and Bhattacharjee, S. Motion of a spherical particle in a cylindrical channel using arbitrary lagrangian–eulerian method. *Journal of colloid and interface science 317*, 2 (2008), 620–630.

[41] Quinn, J., Anderson, J., Ho, W., and Petzny, W. Model pores of molecular dimension: the preparation and characterization of track-etched membranes. *Biophysical journal 12*, 8 (1972), 990–1007.

[42] Reddy, J. N. *An introduction to the finite element method*, vol. 2. McGraw-Hill New York, 1993.

[43] Secomb, T. Flow-dependent rheological properties of blood in capillaries. *Microvascular research 34*, 1 (1987), 46–58.

[44] Secomb, T., Skalak, R., Özkaya, N., and Gross, J. Flow of axisymmetric red blood cells in narrow capillaries. *Journal of Fluid Mechanics 163* (1986), 405–423.

[45] Secomb, T. W. Mechanics of blood flow in the microcirculation. *Biomedical Flows at Low Reynolds Numbers* (1995), 9.

[46] Secomb, T. W., Styp-Rekowska, B., and Pries, A. R. Two-dimensional simulation of red blood cell deformation and lateral migration in microvessels. *Annals of biomedical engineering 35*, 5 (2007), 755–765.

[47] Smith III, F. G., and Deen, W. Electrostatic double-layer interactions for spherical colloids in cylindrical pores. *Journal of Colloid and Interface Science 78*, 2 (1980), 444–465.

[48] Smith III, F. G., and Deen, W. Electrostatic effects on the partitioning of spherical colloids between dilute bulk solution and cylindrical pores. *Journal of Colloid and Interface Science 91*, 2 (1983), 571–590.

[49] Vink, H., Wieringa, P., and Spaan, J. Evidence that cell surface charge reduction modifes capillary red cell velocity-flux relationships in hamster cremaster muscle. *The Journal of physiology 489*, Pt 1 (1995), 193–201.

[50] White, F. M., and Corfield, I. *Viscous fluid flow*, vol. 2. McGraw-Hill New York, 1991.

[51] Zhang, X., Curry, F.-R., and Weinbaum, S. Mechanism of osmotic flow in a periodic fiber array. *American Journal of Physiology-Heart and Circulatory Physiology 290*, 2 (2006), H844–H852.